
UNIVERSITÀ
DI PAVIA

PHD PROGRAM IN EXPERIMENTAL MEDICINE

# A Pre-clinical Study on the Use of the Proprotein Convertase Subtilisin/Kexin type 9 Inhibitor PEP 2-8 to Mitigate Ischemic Injury in a Rat Marginal Donor Model

By

**Tefik Islami**

*Thesis submitted for the degree of Doctor of Philosophy in Experimental Medicine*
*XXXVIII cycle*

**Supervisors:** Prof. Teresa Rampino
Dr. Marilena Gregorini
**The head of PhD program:** Prof. Stefano Perlini

**Declaration**

I hereby declare that, unless explicitly stated otherwise, the content of this dissertation is entirely original and has been submitted and accepted for publication on *International Journal of Molecular Science (MDPI).*

This dissertation is the result of a collaborative effort, carried out in close partnership between my own research activities and the dedicated, unconditional contributions of my colleagues within the Research Unit.

Additionally, I confirm that this thesis has been conducted using the methods and resources detailed within the document. No portion of this work has been presented to any other examining committee. All sources, references, and external contributions, including direct and paraphrased citations, have been duly acknowledged.

## Disclosure

During the preparation of this dissertation, AI-assisted tools were used exclusively to improve language quality and clarity. All content was subsequently reviewed and edited by me, and I take full responsibility for the final version of this work.


## Founding

The present research work funded by the *Italian Ministry of Health* (RC-2018 grant #08054218).

# *Contents*

## List of abbreviations

ADMA: Asymmetric dimethylarginine

Adohcy: S-adenosyl homocysteine

ADP: Adenosine diphosphate

AMP: Adenosine monophosphate

AST: Aspartate aminotransferase

ATP: Adenosine Triphosphate

B6: Vitamin B6

BBF: Bleb formation

BBL: Brush border loss

BHMT: Betaine homocysteine methyltransferase

CBS: Cystathionine βsynthase

cDNA: Complementary deoxyribonucleic acid

CSE: Cystathionine γ-lyase,

CTRL: Control group. Kidneys perfused with Perf-Gen solution

DBD: Donation after brain death

DCD: Donation after circulatory death

DDAH: Dimethylarginine dimethylaminohydrolase

DMSO: Dimethyl sulfoxide

DGF: Delayed graft function

DNA: Deoxyribonucleic acid

ECD: Expanded criteria donors

ESKD: End stage kidney disease

ELISA: Enzyme-linked immunosorbent assay

FC: Fold change

FFPE: Formalin-fixed paraffin-embedded

GS: Glutathione synthase

GSH: Glutathione

H-FABP: Heart-type fatty acid binding protein

H2S: Hydrogen sulfide

HMP: Hypothermic machine perfusion

HP: Hypothermic perfusion

HRP: Horseradish peroxidase

HUVECs: Human umbilical vein endothelial cells.

IQR: interquartile range

IRI: Ischemia-reperfusion injury

LDH: Lactate dehydrogenase

LDL: Low-density lipoprotein

LDLR: Low-density lipoprotein receptor

MAT: Methionine adenosyltransferase

MP: Machine perfusion

mPTP: mitochondrial permeability transition pore

mRNA: Messenger ribonucleic acid

NADPH: Nicotinamide adenine dinucleotide phosphate

NAG: N-acetyl-β-D-glucosaminidase

NMP: Normothermic machine perfusion

NMR: Nuclear magnetic resonance

NO: Nitric oxide

Norm T: Normal tubules

NOS: Nitric oxide synthase

NOX4: NADPH oxidase 4

N-Tyr: Nitrotyrosine

OCT: Optimal cutting temperature compound

PLA2: Phospholipase A2

PBS: Phosphate-buffered saline

PCA: Principal component analysis

PCNA: Proliferation cell nuclear antigen

PCSK9: Proprotein convertase subtilisin/Kexin type 9

PCSK9i: Proprotein convertase subtilisin/Kexin type 9 inhibitor

PEP 2-8: Treated group. Kidneys perfused with Perf-Gen solution supplemented with a PCSK9 inhibitor.

PIPOX: Pipecolate oxidase

qPCR: Quantitative polymerase chain reaction

RNA: Ribonucleic acid

ROS: Reactive oxygen species

RAAS: Renin-angiotensin-aldosterone system

RT-PCR: Real time polymerase chain reaction

SAHH: S-adenosyl homocysteine hydrolase

SCS: Static cold storage

SD: Standard deviation

SEM: Standard error of the mean

TF: Tubular epithelial cell flattening

TID: Tubular ischemic damage

TN: Tubular necrosis

TO: Tubular lumen obstruction

TPI: Tubular cell proliferation index

TSP: 3-trimethylsilyl-propionic-2,2,3,3-$d_4$ acid sodium salt

β2-m: β2-microglobulin

## List of figures

# 1. Introduction

## *1.1 Kidney transplantation*

Kidney transplantation is known as the eligible therapy intervention for patients affected by end-stage renal disease (ESRD), offering a significant survival advantage and improved quality of life when compared with dialysis-based renal replacement therapies. However, the clinical success and long-term outcomes of kidney transplantation are frequently undermined by ischemia-reperfusion injury (IRI), a pathophysiological process that exerts a profound impact on graft function and survival. This is particularly evident in organs procured from expanded criteria donors (ECD) and donors after circulatory death (DCD), both of which are utilized in clinical practice as part of strategies aimed at expanding the donor pool and addressing the critical shortage of transplantable kidneys[1].

In recent years, the utilization of DCD kidneys has risen markedly at the international level, accounting for up to 40% of transplant procedures in some healthcare systems[2]. This expansion reflects an urgent and ongoing effort to reduce the disparity between the growing demand for kidney transplantation and the limited availability of suitable donor organs. Nonetheless, despite their increasing clinical relevance, kidneys retrieved from DCD donors continue to present significant challenges. Reported discard rates for these grafts remain high, ranging between 3% and 33%, largely due to persistent concerns regarding susceptibility to IRI and doubts about overall graft quality[2,3].

From a clinical perspective, kidneys obtained from DCD donors exhibit a higher incidence of delayed graft function (DGF) compared with grafts from donation after brain death (DBD). Although DGF is generally a manageable complication and has only a limited effect on long-term graft survival, its occurrence is not inconsequential, as it contributes to prolonged hospitalization, increased healthcare resource utilization, and greater exposure to immunological risk[4]. Furthermore, ischemic

injury not only predisposes to DGF, but also increases the likelihood of more severe adverse outcomes, including primary non-function (PNF) and heightened rates of acute rejection, both of which negatively influence graft prognosis[1,4] (Figure 1).

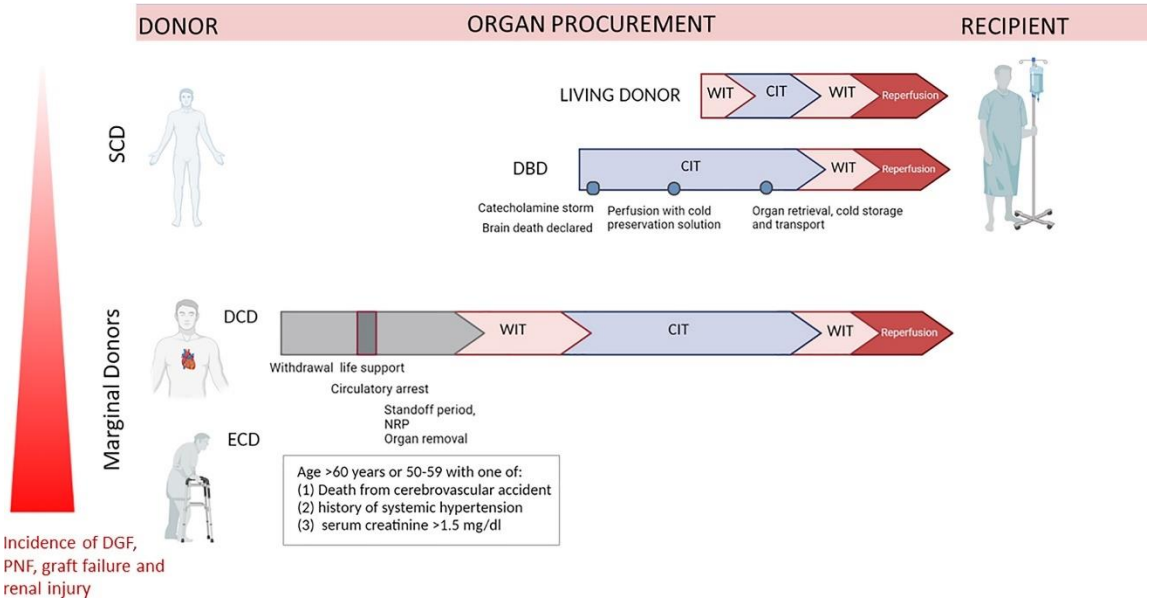


*Figure 1. Representation of different ischemia types exposure of organs retrieved from Living Donor (LD), DBD, DCD and ECD (Franzin R et al)[5]*

Given the rising dependence on marginal donors such as ECD and DCD, IRI remains one of the foremost challenges in kidney transplantation. Addressing this problem is essential for improving organ utilization, reducing discard rates, and ultimately enhancing graft survival.

Current research efforts are focused on the development of novel preservation methods, optimization of peri-transplant management, and implementation of targeted therapeutic strategies aimed at minimizing ischemic injury and its downstream immunological consequences[1,3,4]. Despite significant advances in recent years, further investigation and innovation are required to achieve a more consistent and reliable integration of marginal donor kidneys into clinical practice. This will,

reduce the reliance on organ discard and better meet the needs of patients awaiting transplantation.

### *1.2 Ischemia-reperfusion injury in kidney transplantation*

IRI represents an inevitable and clinically relevant insult in the context of organ transplantation, occurring during both organ procurement and engraftment. Ischemia is initiated when blood flow to an organ is interrupted, resulting in the deprivation of oxygen and essential nutrients. While restoration of blood flow is indispensable to prevent irreversible hypoxic damage, paradoxically, reperfusion itself introduces an additional layer of injury, largely mediated by oxidative stress and inflammatory cascades, thereby amplifying overall tissue damage[6,7].

The extent of ischemic insult varies with the type of donor. In DBD, the warm ischemia period is generally short, typically <30 minutes. By contrast, in DCD, warm ischemia may extend up to 90 minutes, thereby exposing the organ to a significantly greater risk of ischemic injury. Furthermore, transplantation procedures necessitate an obligatory period of cold storage, which, although designed to slow cellular metabolism and mitigate ongoing ischemic damage, may last for several hours and contribute to additional cold ischemia–induced injury[8].

Clinically, IRI has profound implications. It contributes to systemic inflammation, increases graft immunogenicity, and is strongly associated with DGF, acute rejection, and chronic allograft dysfunction. Moreover, IRI is linked to increased morbidity and mortality, as well as prolonged hospital stays, underscoring its importance as a major determinant of transplant outcomes[9,10].

### *1.2.1 Pathophysiology of Ischemia-reperfusion Injury*

The pathogenesis of IRI can be divided into two distinct phases: the ischemic phase, characterized by interruption of blood supply following arterial clamping and organ retrieval, and the reperfusion phase, during which restoration of circulation paradoxically exacerbates tissue injury (Figure. 2)[11].

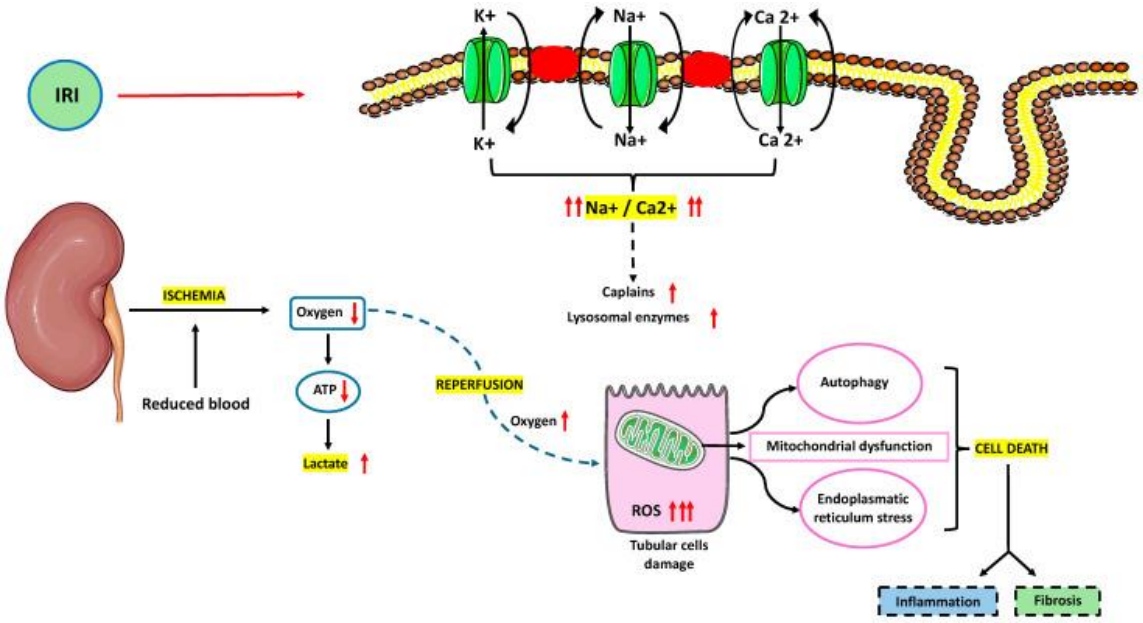


*Figure 2. Pathophysiology of ischemia–reperfusion injury (IRI) (Lasorsa et al.)*

#### *1.2.1.1 Ischemic Phase*

During the ischemic phase, oxygen deprivation leads to a rapid shift from aerobic to anaerobic metabolism, with a consequent inhibition of oxidative phosphorylation and a precipitous decline in intracellular adenosine triphosphate (ATP) production. As a result, lactate accumulates as the predominant energy substrate, causing intracellular acidosis and disruption of ionic homeostasis. Proton accumulation

destabilizes cell membranes, leading to lysosomal enzyme leakage and inhibition of critical ionic pumps. Notably, $Na^+/K^+$ ATPase dysfunction results in intracellular sodium retention, osmotic water influx, and cellular swelling[11,12].

In parallel, impaired calcium homeostasis plays a central role. The loss of normal calcium extrusion mechanisms leads to intracellular $Ca^{2+}$ overload, which in turn activates proteolytic enzymes such as both calpains and phospholipases. These enzymes disrupt cytoskeletal integrity, compromise tight junctions, and initiate pathways of irreversible cell injury[13,14].

ATP degradation compounds this process further. During prolonged ischemia, ATP is sequentially broken down into ADP, AMP, adenosine, inosine, and hypoxanthine. Because adenine nucleotides diffuse outside the cell, the resynthesis of ATP is effectively blocked[15]. Accumulated hypoxanthine becomes a substrate for xanthine oxidase upon reperfusion, promoting reactive oxygen species (ROS) generation and priming the tissue for oxidative injury[16].

Additionally, ischemia is associated with activation of the renin-angiotensin-aldosterone system (RAAS), which exacerbates tissue damage by stimulating macrophage activation, promoting ROS production, and inducing apoptosis and tubular atrophy[17]. Morphologically, ischemic insult initially manifests as sublethal tubular epithelial cell injury with loss of brush borders, polarity disruption, and cytoskeletal damage. In sustained ischemia, the injury progresses to detachment of epithelial cells, cast formation, luminal obstruction, and ultimately cell death[18].

#### *1.2.1.2 Reperfusion Phase*

Although reperfusion is essential to re-establish oxygen supply, it paradoxically intensifies tissue damage. The sudden influx of oxygen results in excessive generation of ROS, mitochondrial dysfunction, and membrane peroxidation, accompanied by recruitment of immune and inflammatory cells. These processes collectively activate

programmed cell death pathways such as apoptosis, necrosis, pyroptosis, and autophagy[6,19].

A critical event in this phase is the activation of xanthine oxidase, which had been synthesized but remained inactive during ischemia. Upon reoxygenation, xanthine oxidase catalyzes the conversion of hypoxanthine to xanthine and uric acid, generating abundant ROS. These free radicals damage mitochondrial, lysosomal, and plasma membranes, exacerbating cell injury[20,21].

ROS also activate phospholipase A2 (PLA2), which generates arachidonic acid metabolites and pro-inflammatory mediators. This cascade enhances leukocyte activation, promotes chemotaxis, and upregulates adhesion molecules that facilitate neutrophil rolling and adhesion to the endothelium. Concurrently, caspase-1 is activated, leading to the release of pro-inflammatory cytokines such as TNF-α and multiple interleukins (IL-1, IL-2, IL-8, IL-10, IL-18), thereby amplifying the inflammatory response[22,23].

The interplay between oxidative stress and calcium overload is particularly deleterious. Elevated mitochondrial calcium concentrations promote opening of the mitochondrial permeability transition pore (mPTP), leading to the release of cytochrome c, succinate, and mitochondrial DNA into the cytosol. These molecules trigger apoptosis, necrosis, and other regulated cell death pathways[14]. Additionally, normalization of pH during reperfusion contributes to further calcium influx, exacerbating calpain activation and accelerating cell structural breakdown[12].

Reperfusion transforms sublethal ischemic injury into irreversible damage. This cumulative insult contributes to impaired graft recovery, particularly in marginal kidneys such as those retrieved from ECD and DCD, thereby emphasizing the critical importance of strategies aimed at mitigating IRI in transplantation (Figure. 3).

*Figure 3. Molecular mechanisms of renal IRI (Franzin R et al)*[5]

## 1.3 Organ Preservation Strategies to Mitigate Ischemic Injury

Preserving the viability of donor kidneys and protecting them from ischemic and hypoxic damage during the pre-transplant period represents a critical determinant of post-transplant outcomes. The increasing reliance on marginal organs, including DCD and ECD, has underscored the need for more advanced methods of preservation and reconditioning that go beyond conventional approaches[24].

Historically, since the 1970s, the standard technique for kidney preservation has been static cold storage (SCS), which involves placing the organ in an insulated container on ice at low temperatures to reduce metabolism and oxygen consumption[25,26]. The rationale behind hypothermia is that decreasing temperature slows cellular metabolic processes, thereby extending graft viability in the absence of oxygen and metabolic substrates. While the protective mechanisms of hypothermia are not fully elucidated, it is well established that the rates of biochemical reactions are temperature-dependent, and cooling effectively prolongs the tolerance of organs to ischemic conditions[24,27].

To enhance the protective effects of hypothermia, cold preservation solutions were developed with key objectives: minimizing cellular swelling, preventing interstitial edema and intracellular acidosis, reducing oxidative stress, and providing substrates necessary for high-energy phosphate regeneration upon reperfusion[27]. Despite these benefits, SCS remains a passive approach that does not allow for real-time assessment of graft quality, nor does it provide opportunities to actively intervene against IRI.

The growing need to expand the donor pool and safely utilize borderline grafts has accelerated the development of machine perfusion (MP) technologies. Unlike static preservation, MP introduces a dynamic system in which perfusion solutions continuously circulate through the renal vasculature, enabling improved oxygenation, nutrient delivery, and waste removal during the ex situ phase of transplantation[28]. This dynamic approach provides several advantages: continuous

flushing of toxic metabolites, prevention of tissue edema, maintenance of vascular integrity, and the possibility to monitor real-time functional and biochemical markers such as intrarenal resistance, perfusion flow, and biomarkers of tubular injury, including lactate dehydrogenase (LDH), aspartate aminotransferase (AST), N-acetyl-β-D-glucosaminidase (NAG), and heart-type fatty acid binding protein (H-FABP)[29]. These parameters aid clinicians in evaluating graft viability prior to implantation, reducing the risk of discarding potentially transplantable organs.

Another major advantage of machine perfusion is that it provides a platform for therapeutic interventions directly to the graft during preservation. This method enables the targeted administration of protective agents, therapeutic gases, stem cells, gene therapies, and nanoparticles without systemic exposure[30]. Such strategies hold promise for actively repairing ischemic or high-risk kidneys, making MP particularly attractive in the setting of ECD and DCD transplantation.

Several modes of MP have been developed, primarily differing by the temperature range and composition of the perfusate. These include hypothermic machine perfusion (HMP), normothermic machine perfusion (NMP), and more recently, strategies involving controlled rewarming under hypothermic to normothermic conditions[31].

### *1.3.1 Hypothermic Machine Perfusion*

HMP involves the circulation of preservation solution at low temperatures (2–8 °C) and represents the most extensively studied form of dynamic preservation, particularly for DCD kidneys[24]. Beyond the metabolic reduction achieved by cooling, HMP provides pulsatile flow that enhances endothelial nitric oxide production, reduces intrarenal vascular resistance, and prevents microvascular obstruction. Evidence suggests that HMP can improve early graft function and reduce the DGF incidence by attenuating IRI and apoptosis. However, its long-term impact on graft

and patient survival remains debate, as several meta-analyses have failed to demonstrate consistent improvements in PNF, acute rejection, or long-term outcomes despite reductions in DGF[28,32].

### *1.3.2 Normothermic Machine Perfusion*

NMP maintains the kidneys under near-physiological conditions by circulating a warmed (35–37 °C), oxygenated, and nutrient-rich perfusate, typically incorporating a red blood cell–based oxygen carrier[32,33]. By preserving metabolic activity and restoring ATP levels, NMP not only avoids cold ischemic injury but also allows real-time functional assessment of renal performance through urine output and metabolic markers. Moreover, it creates a therapeutic window during which interventions to repair the graft can be administered. Several studies suggest that NMP reduces DGF and improves early post-transplant outcomes compared with prolonged SCS[33]. Nevertheless, challenges remain regarding its optimal duration, the ideal perfusate composition, cost-effectiveness, and technological complexity[28].

Taken together, the integration of MP strategies into clinical practice represents a paradigm shift in kidney transplantation. By transforming organ preservation from a passive to an active process, MP not only mitigates ischemic injury but also enables the assessment, repair, and optimization of donor kidneys prior to implantation. These innovations hold particular promise for improving the utilization of marginal grafts and reducing discard rates, thereby expanding the donor pool and ultimately improving patient outcomes[34,35].

### *1.4 PCSK9 in Renal Ischemia–Reperfusion Injury*

In a previous experimental study using a rat model of renal IRI, we observed a marked and early upregulation of proprotein convertase subtilisin/kexin type 9 (PCSK9) following reperfusion, suggesting a previously unrecognized role for this enzyme in renal IRI pathogenesis[37]. This phenomenon is not restricted to the kidney: similar findings have been reported in models of myocardial[38–40], hepatic[41], and cerebral ischemia-reperfusion[42–44]. Importantly, across these different organs, PCSK9 inhibition consistently attenuated structural and functional injury. This identifies PCSK9 as a central mediator of ischemic tissue damage with a potentially conserved pathophysiological role across organ systems.

#### *1.4.1 Biological Functions of PCSK9 Beyond Lipid Regulation*

PCSK9 is a secreted serine protease most commonly associated with lipid metabolism. It binds to the low-density lipoprotein receptor (LDLR), promoting its lysosomal degradation and thereby reducing receptor availability for low density lipoprotein (LDL) clearance. The net effect is an increase in circulating LDL cholesterol, particularly oxidized LDL, a recognized contributor to vascular dysfunction and dyslipidemia[45–47]. Although the liver is the primary site of PCSK9 synthesis, the enzyme is also expressed in extrahepatic tissues including the kidney, intestines, pancreas, lungs, and central nervous system, suggesting a broader biological role[47,48] (Figure. 4).

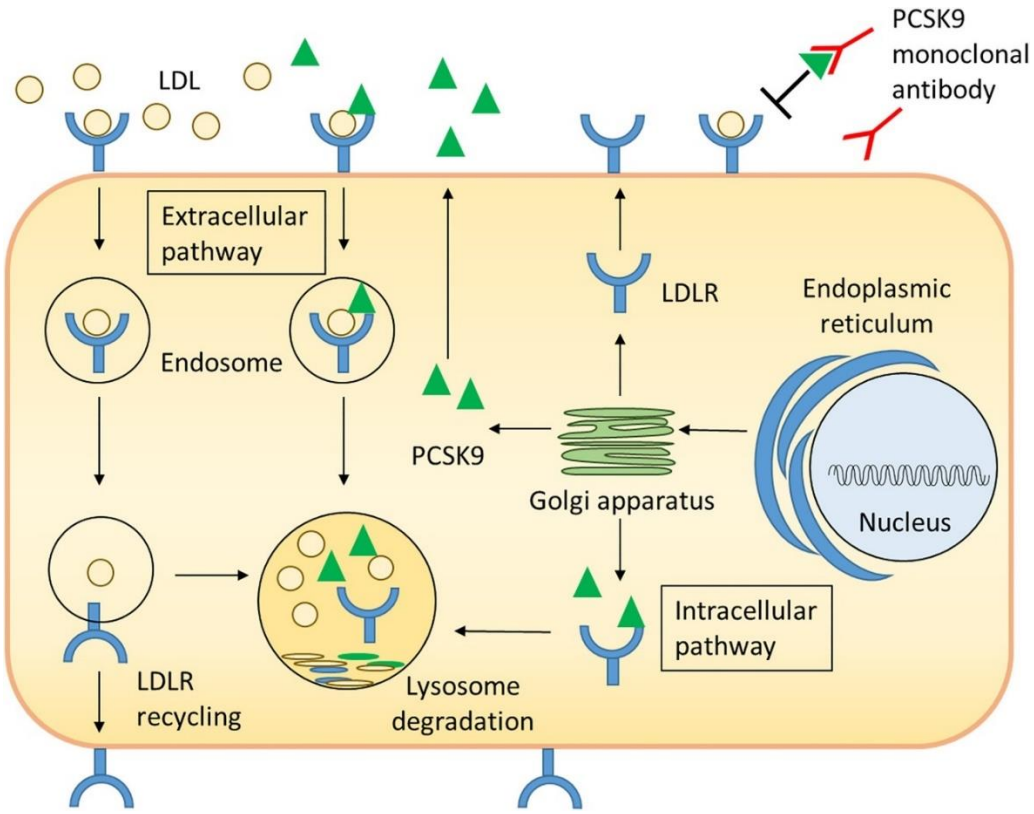


*Figure 4. PCSK9 mechanism of action and PCSK9 monoclonal antibody. The secreted PCSK9 from Golgi apparatus can be sorted directly to lysosomes as a PCSK9–LDLR complex or be secreted into the plasma and then internalized with LDLR to intracellular degradation. PCSK9 promotes the degradation of LDLR in both intracellular and extracellular pathways, resulting in the reduction of LDL clearance from the circulation. PCSK9 monoclonal antibodies inhibit the binding between PCSK9 and LDLR extracellularly (Nishikido T, et al)[36].*

Over the past two decades, proprotein convertase subtilisin/kexin type 9 (PCSK9) has been the subject of intensive investigation in both clinical and translational settings, particularly regarding its role in the pathophysiology of metabolic syndrome and atherosclerotic cardiovascular disease[49,50]. The clinical use of PCSK9 inhibitors (PCSK9i) has revolutionized lipid-lowering therapy, demonstrating not only dramatic reductions in LDL cholesterol but also decreased cardiovascular risk, improved endothelial function, and even attenuation of hepatic steatosis[51–57]. These pleiotropic benefits strongly suggest that PCSK9 plays a pivotal role in multiple interconnected metabolic and inflammatory pathways.

### *1.4.2 PCSK9 as a Mediator of Inflammation, Oxidative Stress, and Mitochondrial Dysfunction*

Beyond cholesterol regulation, PCSK9 has is an important modulator of inflammation and oxidative stress. Its expression is induced by lipopolysaccharides, tumor necrosis factor-alpha, and ROS, implicating it in pro-inflammatory signaling cascades[58,59]. Evidence from both in vitro and in vivo studies suggests that PCSK9 directly contributes to mitochondrial dysfunction and DNA damage, promoting cellular injury in a variety of disease contexts[58–63].

Moreover, PCSK9 has been implicated in programmed cell death pathways, including pyroptosis[60,61]. By driving mitochondrial dysfunction, PCSK9 amplifies oxidative stress and inflammatory signaling, thereby exacerbating ischemia-related injury. In models of fibrosis and chronic tissue injury, PCSK9 silencing preserved mitochondrial function, reduced bioenergetic collapse, and maintained tissue integrity[62,63]. Collectively, these findings highlight PCSK9 as a key upstream regulator of mitochondrial health and a potential therapeutic target for ischemic and inflammatory diseases.

### *1.4.3 PCSK9 in Ischemia–Reperfusion Injury: Translational Perspectives*

A convergence of evidence from renal, cardiac, hepatic, and cerebral IRI models supports the hypothesis that PCSK9 is an important amplifier of ischemic injury. During ischemia, metabolic stress and inflammatory signaling lead to increased PCSK9 expression, which worsens endothelial dysfunction, augments oxidized LDL accumulation, and amplifies ROS-mediated damage. Upon reperfusion, these effects are intensified, as PCSK9 contributes to mitochondrial destabilization, apoptosis, and pyroptotic cell death, thereby further exacerbating organ dysfunction[37–42,44,58–61,64–70].

These mechanistic insights are particularly relevant in the context of organ transplantation, where IRI remains a critical determinant of DGF, long-term graft survival, and patient outcomes. Thus, targeting PCSK9 during the peri-transplant phase may represent a novel strategy to mitigate ischemic injury and improve transplantation success.

### *1.4.4 PCSK9 Inhibition as a Strategy for Ischemic Protection*

PCSK9i, originally developed as lipid-a lowering-therapies, are now recognized to have broader protective effects. In models of myocardial infarction and vascular surgery, PCSK9 inhibition reduced infarct size, improved myocardial contractility, and suppressed autophagy and apoptosis[38–40,52,53]. Similarly, in hepatic IRI, blockade of PCSK9 promoted mitophagy via the Pink1–Parkin pathway, thereby preserving mitochondrial function and reducing hepatocellular injury[64]. In cerebral ischemia models, PCSK9 inhibition alleviated neuronal inflammation, reduced amyloid beta aggregation, and limited infarct volume[42–44].

Notably, the ex vivo organ perfusion setting, including HMP and NMP offers an ideal platform for PCSK9i targeted delivery directly to donor kidneys. This approach allows localized drug exposure without systemic side effects, with the potential to reduce oxidative stress, preserve mitochondrial activity, and enhance graft recovery before implantation. By incorporating PCSK9i into MP protocols, it may be possible to improve outcomes particularly for ECD and DCD kidneys, which are highly susceptible to ischemic injury.

These findings provide a strong translational rationale for exploring PCSK9 inhibition as a novel therapeutic strategy to attenuate IRI, enhance the utilization of marginal kidneys, and ultimately improve renal transplantation success.

## 2. Study Aims

The growing use of kidneys from marginal donors, including DCD, underscores the need for strategies to reduce IRI, which remains a key factor in early graft dysfunction and long-term transplant outcomes. Despite improvements in organ preservation, ischemic damage during procurement and storage continues to limit optimal kidney utilization. Accordingly, the present study was designed to explore whether pharmacological modulation of PCSK9 could represent a promising therapeutic avenue to attenuate ischemic injury during ex vivo hypothermic perfusion (HP).
To address this question, we employed PEP 2-8, a synthetic peptide inhibitor specifically designed to interfere with the binding of PCSK9 to the LDLR.

In addition to its lipid-lowering properties, PCSK9 inhibition has been shown in recent experimental studies to exert protective effects in ischemia-reperfusion models of the heart, where treatment significantly improved left ventricular function, reduced infarct size, and ameliorated mitochondrial performance[71]. Structural studies further confirmed that PEP 2-8 effectively disrupts the PCSK9–LDLR interaction, providing a mechanistic basis for its biological efficacy[72]. More recently, additional evidence has linked PCSK9 activity with vascular dysfunction and pro-inflammatory signaling cascades, including TLR4/MyD88/NF-κB and NLRP3 inflammasome pathways, underscoring its broader role in endothelial injury and systemic inflammation[73].

The *primary objective* of this study was to evaluate whether PEP 2-8 administration during HP could reduce ischemia-induced renal injury in rat DCD kidneys, as assessed by functional and biochemical parameters of organ integrity.

The *secondary objective* was to investigate whether such treatment could enhance overall graft viability, thereby improving the suitability of DCD kidneys for transplantation.

No predefined humane endpoints were established given the ex vivo nature of the animal experimental model.

If effective, the pharmacological inhibition of PCSK9 during ex vivo perfusion could provide a dual benefit:

(i) protecting renal tissue from ischemic and inflammatory insults and
(ii) offering a therapeutic platform to actively recondition marginal kidneys before transplantation.

In the long term, this approach may contribute to expanding the donor pool, improving graft utilization, and ultimately enhancing clinical outcomes in kidney transplantation.

## 3. Materials and Methods

Figure 5 illustrates the experimental design of this study. The study was approved by the Animal Care and Use Ethics Committee of the University of Pavia, Italy and by the Italian Ministry of Health (protocol code: 175.2023-PR,03/03/2023). All experimental procedures were conducted in full compliance with the Animal Research: Reporting of In Vivo Experiments (ARRIVE) guidelines[74], ensuring transparency, reproducibility, and adherence to international ethical standards. Animal welfare was prioritized throughout the study, with continuous monitoring and the implementation of humane end-of-life protocols.

All interventions were performed under general anesthesia, causing no significant pain, and were carried out under the supervision of personnel trained in proper animal care and handling. Prior to surgery, animals were housed in approved cages in accordance with current regulations and monitored daily by research staff. Veterinary oversight was maintained throughout the study by the attending veterinarian.

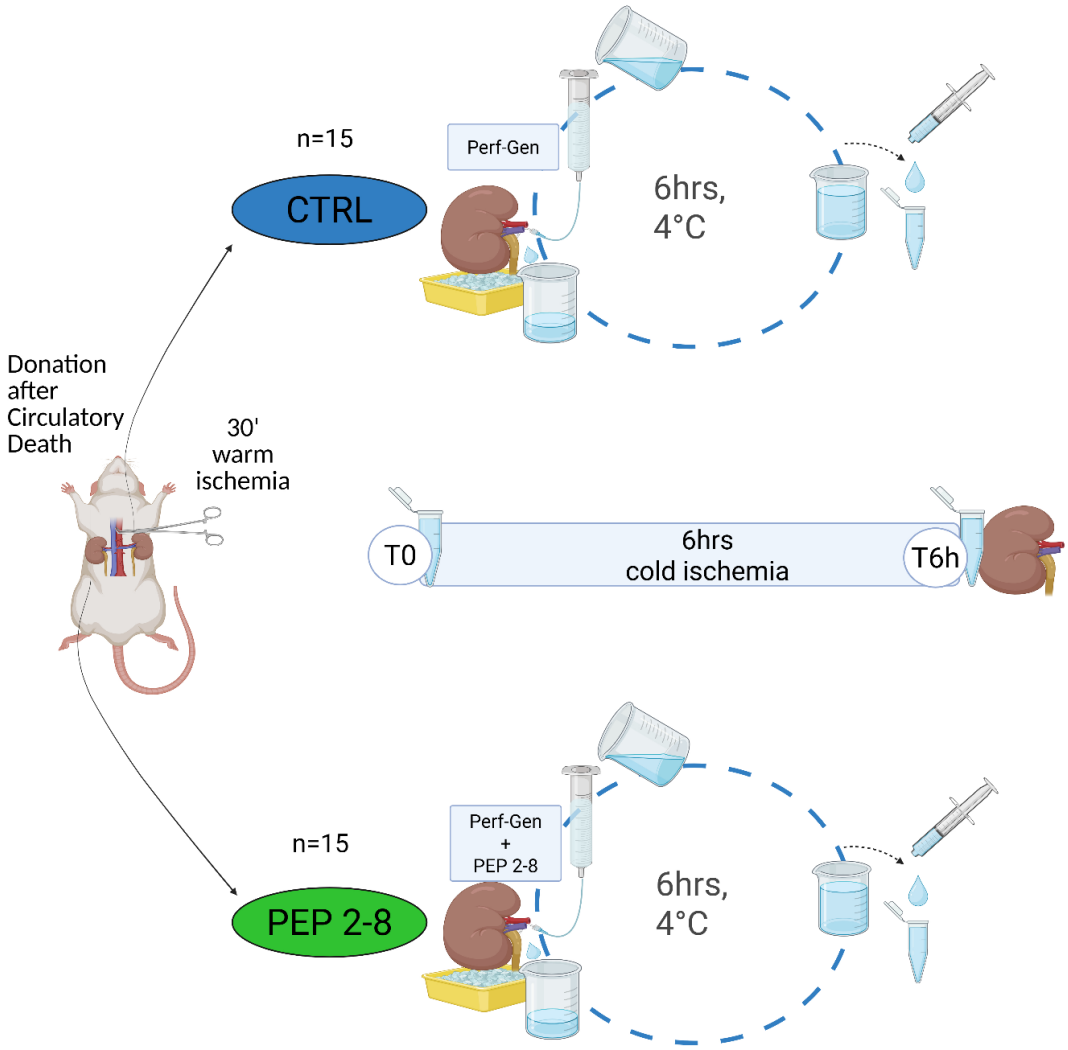


*Figure 5. Experimental Design of the DCD Rat Kidney Perfusion Model. Donation after circulatory death (DCD) was modelled by clamping the rat aorta for 30 minutes. Following this warm ischemia phase, kidneys were subjected to six hours of continuous hypothermic perfusion at 4 °C using either Perf-Gen solution alone (CTRL group, n = 15) or Perf-Gen supplemented with the PCSK9 inhibitor PEP 2-8 (PEP 2-8 group, n = 15). Effluent samples were collected at the onset (T0) and conclusion (T6h) of perfusion, while renal tissues were harvested at T6h for further analysis. Figure created with BioRender.com. Rampino, T. (2025).*

### *3.1. Animal DCD Model*

Male Fischer rats (n=15) (8 weeks old, Harlan Italy s.r.l. Monza, Italy) were used as a DCD model[75]. Under isoflurane anesthesia (2%–5%), a midline laparotomy was performed to expose the retroperitoneal renal areas. The lumbar arteries were isolated and ligated, followed by isolation of the renal arteries and veins. Warm ischemia was induced by clamping the aorta for 30 minutes to simulate DCD conditions. Subsequently, bilateral nephrectomies were performed, preserving the renal hilum. Following nephrectomy, animals were humanely euthanized under anesthesia using approved methods, in accordance with ARRIVE guidelines[74].

Both kidneys from each DCD rat were perfused for 6 hours at 4°C (cold ischemia) using a continuous falling system (HP) and one kidney from each rat was assigned to a treatment arm:

A) CTRL (control group, n=15): Left kidneys perfused with Perf-Gen solution (IGL Group, Lissieu, France)

B) PEP 2-8 (treated group, n=15): Right kidneys perfused with Perf-Gen solution supplemented with PCSK9 inhibitor.

HP was performed using a gravity-driven system. Specifically, 100 mL of perfusion solution, with or without PCSK9i, was used to perfuse the kidney. The solution was delivered through a 100 ml syringe connected to the organ via a perfusion tube. The syringe was positioned at a height of 2.20 meters to achieve a flow rate of 2.5 mL/min and a pressure of 1.81 MPa. each kidney was placed in a Petri dish resting on an ice block to maintain hypothermia.

A cyclical perfusion system was employed whereby effluent was collected in a beaker beneath the kidney and recycled by refilling the syringe, enabling continuous circulation of the perfusate (Fig. 5). PEP 2-8 (10 μM; Sigma-Aldrich, Darmstadt, Germany), a synthetic PCSK9i, was prepared by dissolving the stock compound in 1 mL of dimethyl sulfoxide (DMSO) to a concentration of 1 μg/μL. Serial dilutions

were performed to obtain a working solution of 2.5 µg/100 µL DMSO. Based on prior IRI studies and the average weight of 8-week-old male Fischer rats (~250 g), a final concentration of 3 µg/100 mL Perf-Gen was chosen for kidney perfusion[71,72,76].

In the control group, an equivalent volume of DMSO was added to the Perf-Gen solution to control for any potential vehicle effects.

### 3.2. Samples Collection

At both the start (T0) and end (T6h) of hypothermic perfusion, 1 mL of effluent was collected using a sterile 1 mL syringe to measure glucose and LDH levels.

At T6h, kidneys from each experimental group were divided into three portions: one was fixed in 10% neutral-buffered formalin for histological analysis, another was embedded in optimal cutting temperature (OCT) compound and frozen for subsequent metabolomic studies, and the remaining tissue was snap-frozen in liquid nitrogen and stored at –80 °C for gene expression and biochemical assays.

### 3.3. Tubular Ischemic Damage Score

Twenty subserial cross-sections of formalin-fixed paraffin-embedded (FFPE) renal tissues (n=15 per group) were stained with periodic acid– Schiff (PAS). The tubular ischemic damage (TID) score determined by evaluating all tubules visible in at least 10 non-consecutive, non-overlapping high-power fields as previously described[75].

In tubules examined, epithelial cell flattening (TF), brush border loss (BBL), blebbing (BBF), necrosis (TN), and lumen obstruction (TO) were observed.

TF and BBL were classified as mild lesions and scored as 1, BBF, TN, and TO as severe lesions and were scored as 2. Normal tubules were scored as 0. When ≥2 lesions were present in the same tubule, the highest severity score was assigned.

### 3.4. Tubular Proliferation Index and N-Tyrosine Staining

FFPE sections from 15 control kidneys and from 15 PEP 2-8-treated kidneys were dewaxed in xylene, passed through a graded series of alcohols for clearing, and rehydrated in distilled water. Endogenous peroxidase activity was blocked with 3.7% hydrogen peroxide ($H_2O_2$, v/v in water) followed by a 15-min rinse in H2O. Following three washes in 150 mM PBS, antigen retrieval was performed by microwaving the sections in citrate buffer pH 6 and then incubated overnight at 4 °C with monoclonal mouse anti-proliferating cell nuclear antigen (PCNA) antibody (1:200, Santa Cruz Biotechnology, Santa Cruz, CA, USA) or N-Tyrosine (N-Tyr) antibody (1:100 Santa Cruz Biotechnology, Inc., Dallas, TX, USA). Following three PBS washes, the tissues were treated with the Horseradish Peroxidase (HRP) Goat Anti-Mouse IgG Polymer Detection Kit (IMMPRESS, Vector Laboratories, Inc. Newark, CA, USA) for 45 minutes at room temperature. The immunocomplex was visualized using a biotin-streptavidin-peroxidase system and 3,3-diaminobenzidine (Dako, Glostrup, Denmark). Sections were lightly counterstained with Harris hematoxylin. Negative controls were prepared by omitting the primary anti-body and substituting it with immunoglobulin G (IgG). Ten non-consecutive fields from each immunostained kidney section were analyzed. Images were captured using a Nikon Eclipse E200 microscope equipped with a CCD camera and analyzed with ImageJ soft-ware (NIH). The tubular cell proliferation index (TPI) was calculated as the ratio of nuclei expressing PCNA to the total number of nuclei in each tubule, across all analyzed fields (magnification ×40).

N-tyr expression was evaluated by converting the immunohistochemistry images to black and white and quantifying the number of black pixels using ImageJ software (magnification ×10). Results were expressed as the percentage of black pixels relative to the total pixel count[77].

Both TPI and N-tyrosine expression are reported as median and interquartile range (IQR) of the analyzed fields.

### 3.5. Apoptosis

FFPE sections (5 μm) from 15 control and 15 PEP 2-8 kidneys were deparaffinized, rehydrated, and subsequently treated with 3% hydrogen peroxide in methanol. Following microwave antigen retrieval in 0.1 M sodium citrate, slides were incubated overnight at 4 °C in a humidified chamber with a primary polyclonal antibody against Cleaved Caspase-3 (Asp175) (1:400 dilution in PBS containing 0.05% Tween 20) (Cell Signaling Technology, Euroclone, Milan, Italy). After PBS washes, tissues were incubated with UltraPolymer Goat anti-Rabbit IgG (H&L) conjugated to HRP (ready to use; ImmunoReagents Inc., Microtech, Pozzuoli, Italy) for 45 minutes at room temperature. The immunocomplex was visualized using 3,3-diaminobenzidine (Roche, Microtech). Nuclei were counter-stained with Carazzi's hematoxylin, and apoptosis was examined using a Leica 2500 DM microscope. Negative controls were obtained by omitting the primary antibody and incubating with rabbit IgG (Vector Laboratories, DBA Italia, Segrate, Italy). For each kidney, a total of 1,000 tubular cell nuclei were counted, and results were expressed as the percent-age of positive cells.

### 3.6. RNA Extraction, Reverse Transcriptase, and Polymerase Chain Reaction

Total RNA was extracted from 15 control tissues and 15 PEP-2-8-treated tissues using the TRiFast II reagent (Euroclone) following the manufacturer's guidelines and quantified with a BioPhotometer reader (Eppendorf, Hamburg, Germany). RNA quality was also verified assessed by evaluating the 260/280 and 260/230 absorbance ratios, which should fall within the ranges of 1.8–2.1 and 2.0–2.2, respectively. A total of 110 ng of RNA was reverse transcribed into cDNA using the iScript cDNA Synthesis Kit (Bio-Rad Laborato-ries, Milan, Italy). For quantitative PCR (qPCR), the diluted cDNA was amplified using the LightCycler 96 SW system (Roche, Basel, Switzerland) and Luna Universal qPCR Master Mix (Euroclone) with specific primers. The PCR protocol included an initial denaturation at 95 °C for 120 seconds,

followed by 40 cycles of amplification at 95°C for 10 seconds, 59°C for 30 seconds, and 68°C for 20 seconds. Initially, in accordance with MIQE guidelines, 5 different reference genes were tested: β2-microglobulin (B2M), GAPDH, β-actin, RPLP0, and 18S RNA. Gene expression levels were subsequently calculated as relative quantification using B2M as the reference gene and expressed as fold changes comparing PEP 2-8-treated samples to control kidneys[78,79].

| Gene | Accession Number | Primer Forward 5'→3' | Primer Reverse 5'→3' |
|---|---|---|---|
| Pcsk9 | NM_199253 | CAT GGA ACC TGG AGC GGA TT | ACC TGG CTA CTT CCG TCA GG |
| NOX4 | NM_053524.1 | TTT CTC AGG TGT GCA TGT AGC | GCG TAG GTA GAA GCT GTA ACC A |
| B2M | NM_004048.4 | GGG ACT AAA CCT CCA GCC AC | CTA CAG CAC ACG CAG TCT GA |

*Tabel 1. Gene sequences of: PCKS9 (proprotein Convertase Subtilisin/Kexin type 9), NOX4 (NADPH oxidase 4) and B2M (β2-microglobulin).*

## 3.7. Biochemical Assays

Glucose and lactate levels in effluent fluids were measured using blood gas analysis (GEM Premier 4000, Werfen, Barcelona, Spain). Glucose release was calculated as the percentage increase from baseline glucose concentrations, based on the difference between glucose levels at the start and end of perfusion.

Effluent pyruvate levels were determined by spectrophotometry (Brea, California, USA). Tissue and effluent LDH levels were measured using a Clinical Chemistry

Analyzer (ARCHITECT, Abbott, Italy). Effluent samples were collected as follows: 15 samples from the control group at T0 and T6h, and 15 samples from the PEP 2-8-treated group at both time points.

Tissue adenosine triphosphate (ATP) levels were quantified using an enzyme-linked immunosorbent assay (ELISA) (ab83355, ATP Assay Kit; Abcam, Cambridge, UK) on homogenized tissue samples (n = 15 per group).

## 3.8. Metabolomics Studies

Before analyzing the study samples, the feasibility of performing NMR metabolomics on frozen OCT-embedded biopsies was established by optimizing a protocol for tissue removal from OCT and extraction of hydrophilic metabolites from kidney resections. This optimized protocol was then applied to the 30 study samples (15 from the control group and 15 from the PEP 2-8 group).

To further improve the standard NMR metabolomics workflow, the ASICS approach was implemented for automated metabolite identification and quantification[80,81].

### 3.8.1. Extraction of polar metabolites

To remove OCT, embedded samples were transferred into 14 mL Falcon™ tubes and washed four times with ice-cold PBS, followed by three additional washes with ice-cold $H_2O$, keeping the biopsies on ice between each washing step. Samples were then placed to vials containing ceramic beads (CKMix - 2 mL, Montigny-le-Bretonneux, France) and homogenized in 1 mL of cold MeOH/$H_2O$ (80/20, v/v). The average tissue weight was 171 mg (range 81-257 mg).

Homogenization was performed using a Precellys Evolution Cryolys tissue-lyser (Bertin Technologies) at 4°C with three 15-second cycles at 6800 rpm. The homogenate was then centrifuged at 12,000 rpm for 10 minutes at 4°C, and the

supernatant, containing hydrophilic metabolites, was dried in a Speed Vacuum concentrator (Eppendorf) without heating for 3.5 hours.

### 3.8.2 NMR spectra acquisition and processing

NMR spectra were recorded using a Bruker Avance NEO 700 MHz spectrometer equipped with a TCI CryoProbe (Bruker BioSpin, Karlsruhe, Germany). Data acquisition and processing were performed with the software TOPSPIN 4.1.4 (Bruker BioSpin).

For each sample, one-third of the dried extract was dissolved in 0.2 mL of deuterated phosphate buffer at pH 7.4, containing 50 mM $Na_2HPO_4/NaH_2PO_4$, 0.5 mM $NaN_3$, and 0.2 mM 3-trimethylsilylpropionic-2,2,3,3-$d_4$ acid sodium salt (TSP) as the frequency reference. NMR acquisition began within 30 minutes of reconstitution, with samples kept on ice. A one-dimensional 1H spectrum was acquired at 25 °C using the 1D-1H NOESY (Nuclear Overhauser Effect Spectroscopy) pulse sequence, along with the standard acquisition and processing parameters optimized for metabolomics of biological samples[82,83].

### 3.8.3. Metabolite identification and quantification were performed using ASICS.

The complete ASICS library[80,81] containing 216 reference compounds, was up-loaded alongside with the 30 pre-processed spectra of the metabolic extracts. Spectral regions corresponding to TSP, residual OCT, and water (-0.05 to 0.05 ppm, 3.700 to 3.730 ppm, and 4.700 to 5.100 ppm, respectively) peaks were arbitrarily set to 0.00 intensity. Subsequently, spectra were normalized using the Probabilistic Quotient Normalization approach, with the median spectrum as reference[82,83]. Finally, metabolite identification and quantification were performed using the default ASICS

settings, applying the advanced joint quantification strategy combined with a first step of independent quantification, with a cleaning threshold set at 1%.

### 3.9 Statistical Analysis

Statistical analyses were conducted using GraphPad Prism software (San Diego, CA, USA). Rats were randomized in a 1:1 ratio to receive Perf-Gen Solution with PEP 2-8 in the left kidney and Perf-Gen Solution in the right kidney, or vice versa, with each rat serving as its own control. The sample size was determined based on the primary endpoint (TID) and on the main comparison between CTRL kidneys and PEP 2-8 kidneys, after 6 hours of HP. Due to feasibility, the study included 15 kidneys per group. Assuming 80% power and a two-sided alpha error of 5%, this sample size will allow the detection of an effect size of 1.06 standard deviations, which is considered large according to Cohen's criteria.

Quantitative data are presented as mean ± standard deviation (SD) or standard error of the mean (SEM), median with interquartile range (IQR), minimum and maximum values, or percentages, depending on the data distribution.

Categorical data are presented as frequencies.

Parametric and non-parametric continuous variables between groups were compared using paired t-tests, Wilcoxon tests, or Wilcoxon matched-pairs signed-rank tests, as appropriate. Fisher's exact test was used to compare frequencies.

Relative metabolite concentrations estimated via ASICS were analyzed using Principal Component Analysis (PCA) after scaling to unit variance[84].

Additionally, univariate analyses, including unpaired t-tests and the non-parametric Kruskal-Wallis test, were performed to identify significant differences in metabolite concentrations between PEP 2-8 and control groups.

A p-value of less than 0.05 was considered statistically significant.

# 4. Results

## 4.1. Reduced PCSK9 Gene Expression After Renal Conditioning with PEP 2-8

RT-PCR analysis revealed that kidneys treated with PEP 2-8 exhibited an approximate 30% reduction in PCSK9 mRNA expression compared to paired control (CTRL) ($p<0.05$, paired t-test) (Figure. 6).

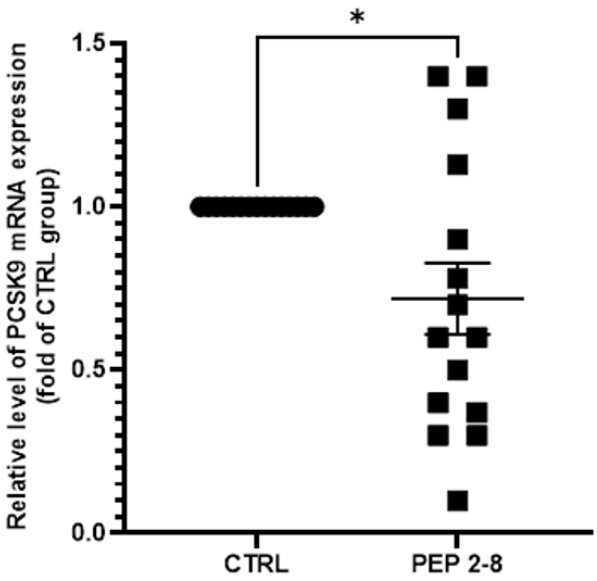


*Figure 6. Effect of PEP 2-8 on PCSK9 gene expression. Real-time polymerase chain reaction (RT-PCR) was conducted to assess PCSK9 gene expression in 15 control kidneys and 15 kidneys perfused under identical conditions, except for the addition of PEP 2-8 to the perfusion solution. All data were analyzed using paired T-test. Gene expression was quantified by relative comparison to the reference gene B2M, and results were expressed as fold changes of PEP 2-8-treated samples relative to their paired controls. The results are presented as means ± SEM. (*p<0.05).*

## 4.2. Reduction in Ischemic Tubular Damage in Kidneys Treated with PCSK9 Inhibitors

Supplementing the Perf-Gen solution with PEP 2-8 conferred significant protection against ischemic tubular damage (median (IQR) CTRL 143.00 (123-165); PEP 2-8 107.00 (82-135); $p<0.001$) (Figure. 7A). Specifically, PEP 2-8 treatment reduced the extent of tubular necrosis (median (IQR): control 12.50% (9.00%-15.75%) vs PEP 2-8 5.50% (3.25%-10.50%); $p<0.001$) while preserving a greater proportion of normal tubular structures compared to controls (median (IQR): control 9.50% (5.50%-12.00%) vs PEP 2-8 29.00% (24.25%-39.50%); $p<0.001$) (Figure. 7B, 7C and 7D).

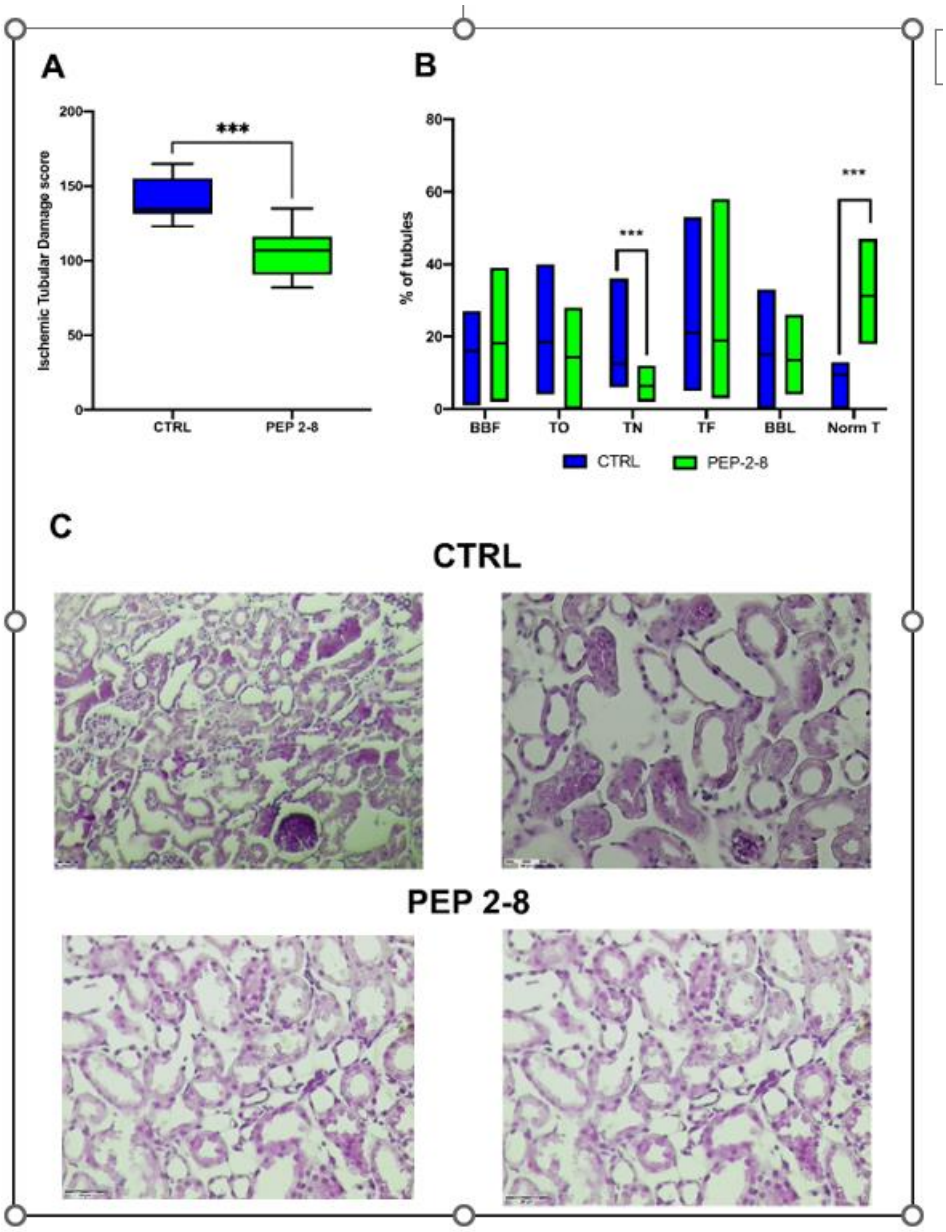


*Figure 7. Renal ischemic damage in control kidneys (CTRL, n=15) compared to PEP 2-8 treated kidneys (PEP 2-8, n=15). (A) Box-plots representing the tubular ischemic damage score expressed as median and 2.5-97.5 percentile and standard deviation (***p<0.001). Data were analyzed using the Wilcoxon test. A total of 10 fields per kidney were evaluated. (B) The graph represents single tubular ischemic lesions in the study groups. Blebbing Formation (BBF) and Tubular Flattening (TF) were considered mild lesions; Tubular Obstruction (TO), Tubular Necrosis (TN) and Brush Border Loss (BBL) were considered severe lesions; Normal Tubules (Norm T) were scored with 0. Data are ex-pressed as percentage of tubules/10 renal fields and analyzed using Multiple Wilcoxon Test (*** p < 0.001). (C). PAS staining of representative renal sections from the CTRL group and (D) PEP 2-8 group at the end of the perfusion (left: 20X, right: 40X magnification).*

Mild lesions were comparable between groups in terms of severity.

These histological findings were corroborated by biochemical markers of tissue injury; LDH levels were significantly lower in the PEP 2-8 group compared to controls. (Median tissue/effluent LDH levels CTRL 811.30 (range: 378.70–1094) versus PEP 2-8 532.80 (range: 266.20–854.00) ($p < 0.05$) (Figure. 8).

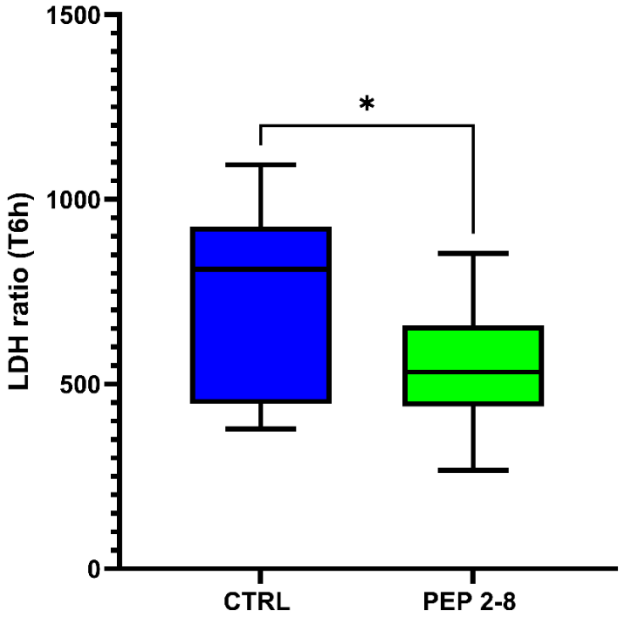


*Figure 8. Comparison between the two groups of LDH levels expressed as ratio between tissue and effluent levels, collected at the end of perfusion. Data are expressed as median and 2.5-97.5 percentile. (* $p < 0.05$).*

### 4.3. Preserved Tubular Regeneration and Reduced Apoptosis in Kidneys Treated with PEP 2-8

To assess tubular regeneration, we measured the expression of Anti-proliferating cell nuclear antigen (PCNA). Kidneys treated with PEP 2-8 showed significantly higher PCNA expression than controls (median (IQR): control 0.61 (0.13–1.65) vs. PEP 2-8 1.96 (0.95–2.58); $p<0.05$) (Figure. 9A). This finding aligns with the greater proportion of preserved tubules observed in the PEP 2-8 group. Furthermore, PEP 2-8 treatment significantly reduced apoptosis. The percentage of kidneys positive cleaved caspase-3, was markedly lower in the PEP 2-8 group compared to controls (control: 56.00% vs. PEP 2-8: 9.00%; $p<0.0001$) (Figure. 9B).

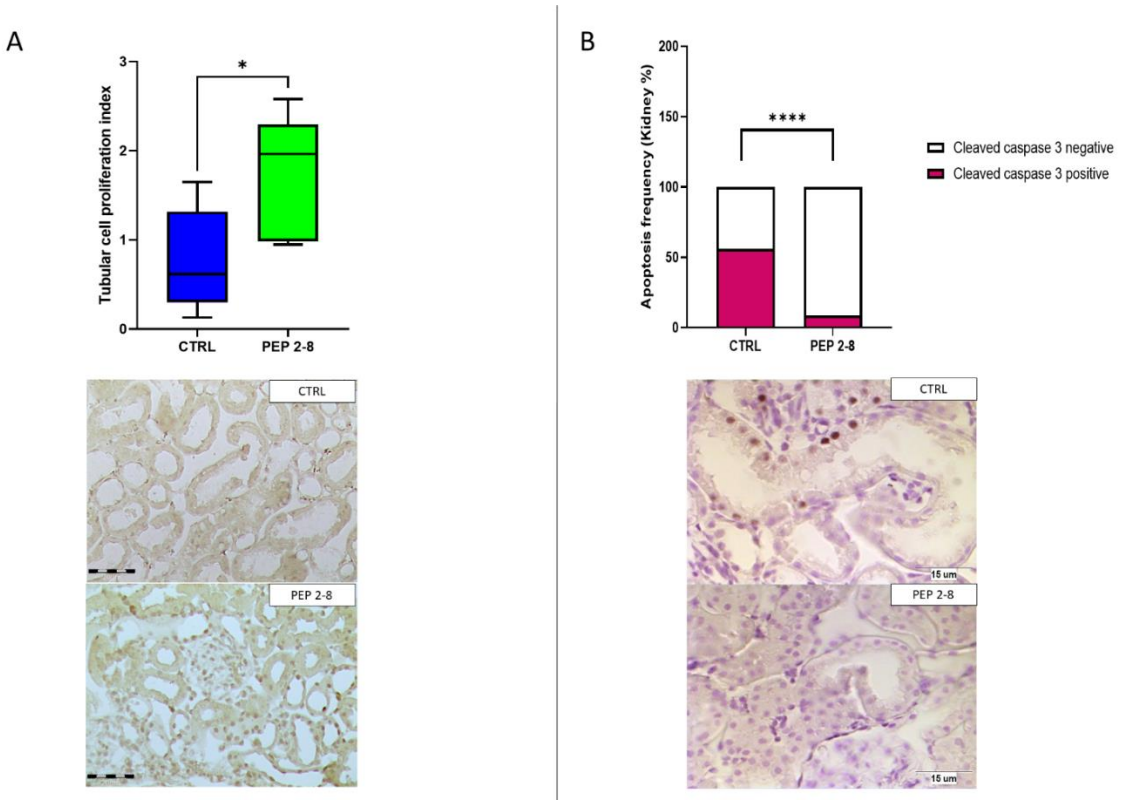


*Figure 9. PEP 2-8 effect on cell proliferation and apoptosis in control kidneys (CTRL, n=15) and PEP 2-8 treated kidneys (PEP 2-8, n=15). (A) Top: Box plots represent tubular proliferation index (TPI). TPI was defined as the ratio between the nuclei expressing PCNA and the total nuclei in each tubule, in ten non-consecutive fields from each immunostained kidney (×40 magnification). Data are expressed as median and 2.5-97.5 percentile. Wilcoxon test was performed to compare data from the two study groups. (*p<0.05) Bottom: Representative sections of PCNA immunostaining (×40 magnification). (B) Top: Apoptosis frequency in the two study groups was assessed by counting a total of 1,000 tubular cell nuclei per kidney. Results are presented as the percentage of kidneys with cleaved caspase-3 positive (pink) or negative (white) staining. Data from the two groups were compared using Fisher's exact test. (****p<0.0001) Bottom: Representative sections of cleaved caspase 3 immunostaining (40x magnification).*

## 4.4. Reduced Oxidative Stress in Kidneys Treated with PEP 2-8

We next evaluated markers of oxidative stress, PEP 2-8 treatment resulted in a significant, approximately 20% downregulation of NADPH oxidase 4 (NOX4) gene expression, compared to controls, key enzyme responsible for generating oxidant molecules ROS implicated in apoptosis and renal damage[85], ($p < 0.05$, CTRL vs. PEP 2-8) (Fig. 10A).

Consistent with this, protein tyrosine nitration, a biomarker of oxidative damage was markedly lower in the PEP 2-8 group than controls, as measured by N-Tyrosine immunostaining (median [IQR]: CTRL 7.46% [5.67%–9.07%] vs. PEP 2-8 2.85% [2.42%–3.31%]; $p < 0.01$) (Fig. 10B).

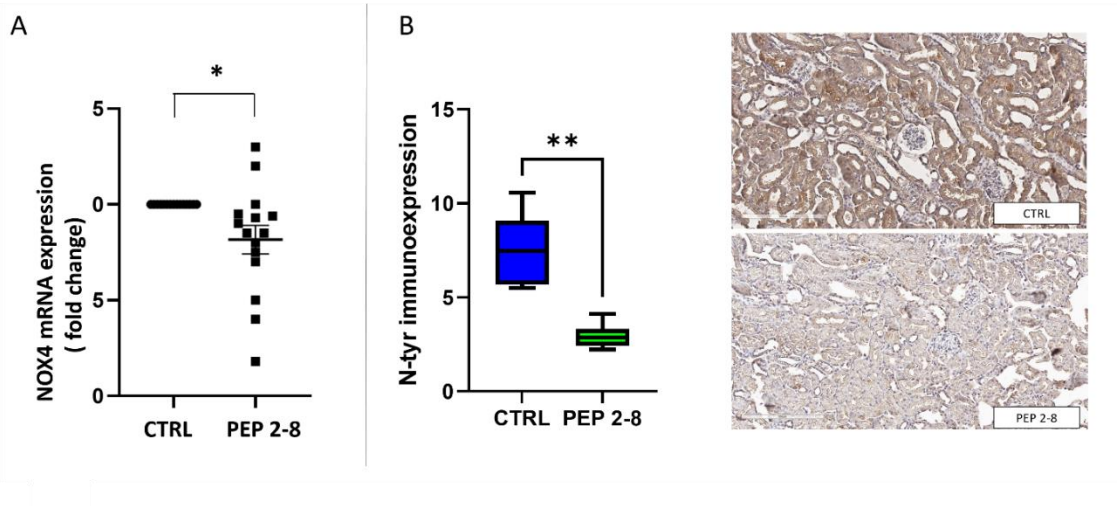


*Figure 10. Markers of oxidative stress in CTRL (n=15) and PEP 2-8 (n=15) groups. (A) NOX4 mRNA expression was measured by quantitative real-time PCR. Results were normalized to β2-microglobulin (β2-m) transcript levels and expressed as fold changes relative to control kidneys (*p < 0.05). (B) N-tyrosine expression was quantified by converting immunohistochemistry images to grayscale and analyzing pixel counts using ImageJ software (10x magnification). Data are ex-pressed as the percentage of black pixels relative to the total pixel count. The left panel shows quantitative analysis of N-tyrosine immunostaining, presented as median, 2.5–97.5 percentile range, and standard deviation. Statistical comparisons between groups were performed using a paired T-test (p < 0.01). Representative images (20× magnification) are shown on the right.*

## 4.5. Sustained Metabolic Activity in Kidneys Treated with PEP 2-8

To assess the tissue energetic status, we measured ATP levels in kidney samples at the end of perfusion period. PEP 2-8-treated kidneys exhibited significantly higher ATP concentrations compared to the control group (mean ± SD: PEP 2-8, 0.03 ± 0.01 nmol/µl vs. CTRL, 0.02 ± 0.01 nmol/µl; $p < 0.05$). In parallel, glucose release in to the effluent fluid, reflecting metabolic activity, was significantly elevated in PEP 2-8-group (median [IQR]: PEP 2-8, 35.48% [12.28%–82.93%] vs. CTRL, 12.26% [7.10%–29.84%]; $p < 0.01$) (Fig. 11). In contrast, lactate and pyruvate concentrations in the effluent did not differ significantly be-tween the two study groups.

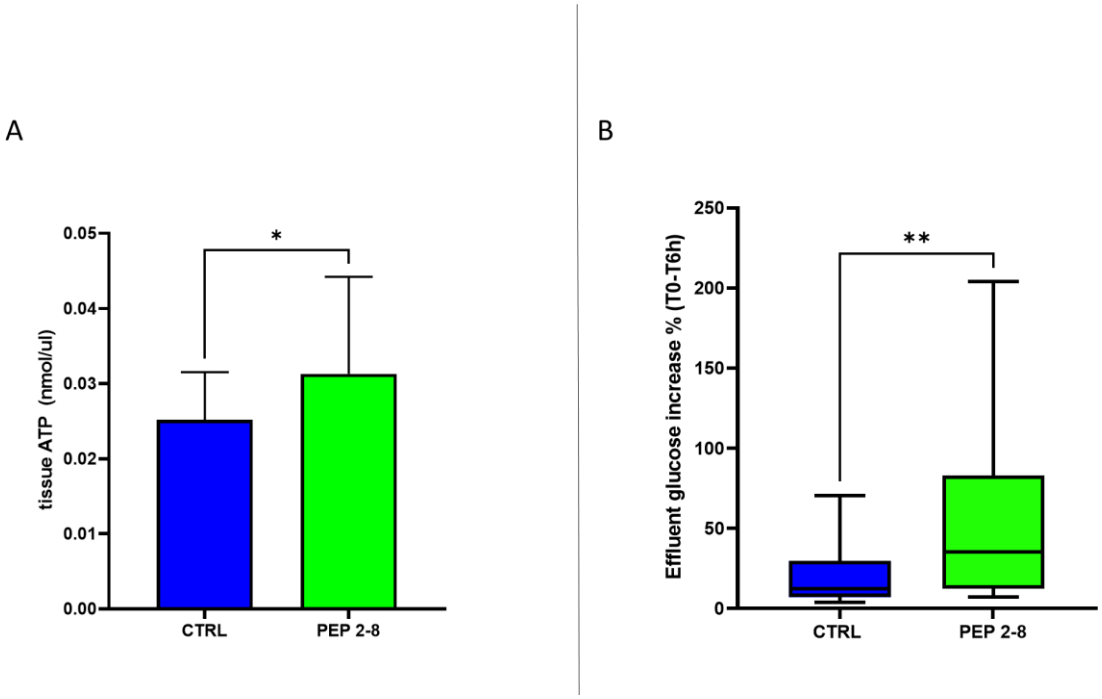


*Figure 11. Effects of PEP 2-8 on ATP and glucose levels in the two study groups (CTRL, n=15; PEP 2-8, n=15). (A) Columns showing the ATP levels (nmol/ul) in the tissue of CTRL and PEP 2-8 groups, compared suing paired T-test. Data are shown as media and standard deviation (*p<0.05). (B) Graph represents the percentage of glucose release in the effluent during the hypothermic perfusion. (**p<0.01). Results were analyzed using Wilcoxon test. Data are expressed as median and 2.5-97.5 percentile.*

## 4.6. Metabolomics Profiles of Treated and Control Kidneys

Untargeted metabolomic analysis identified 167 compounds from the reference metabolite library. The resulting relative concentrations were used for statistical analysis. To investigate overall metabolic trends and assess potential group separation or outliers, we performed Principal Component Analysis (PCA)[84]. The analysis revealed no clear clustering between groups, and the first two principal components accounted for only 45.9% of the total variance, indicating a high degree of similarity in the metabolic profiles of PEP 2-8-treated and control kidneys. (Fig. 12).

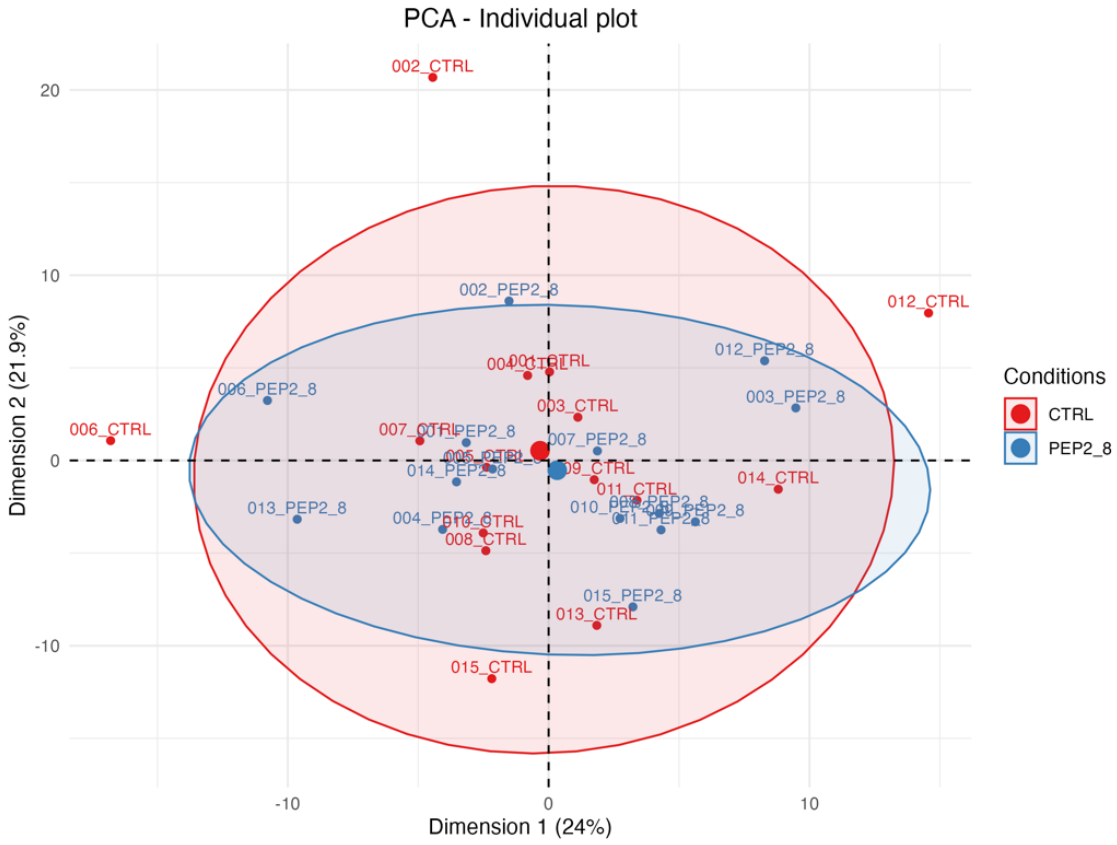


*Figure 12. Bidimensional score plot pf PCA performed on ASICS results relative to 30 samples (15 control and 15 PEP 2-8 samples).*

To identify specific metabolic changes, the concentration data were analyzed using both unpaired t-tests and the non-parametric Kruskal–Wallis test. Across both analyses, only 5 of the 167 detected metabolites showed statistically significant differences between the groups (Table 2 and Figure. 13).

| **Metabolite** | **Kruskal Wallis p Value** | **T Test p Value** |
|---|---|---|
| Dimethylamine | 0.0136 | 0.0047 |
| 2-Oxobutyrate | 0.0152 | 0.0150 |
| L-Carnosine | 0.0213 | 0.0104 |
| Sarcosine | 0.0362 | 0.0358 |
| Biliverdin | 0.0488 | 0.0322 |

*Table 2. Significantly altered metabolites according to univariate statistical tests. The raw p values relative to unpaired t-test and to KruskalWallis test are reported.*

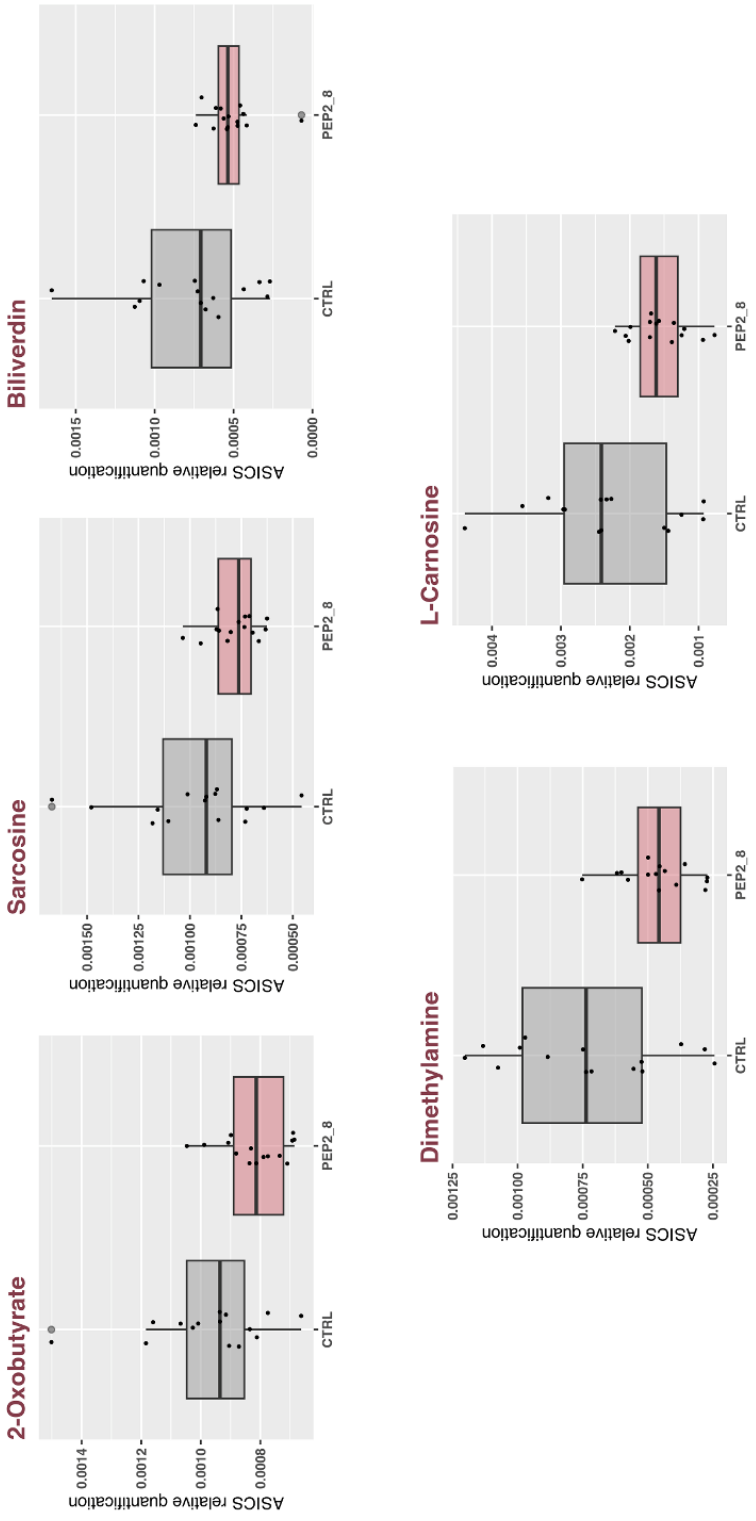


*Figure 13. Box plots of the 5 significantly altered metabolites according to t-test and Kruskall Wallis test, relative to 30 samples (15 control and 15 PEP 2-8 samples).*

## 5. Discussion

In this study, we investigated PCSK9 as a novel therapeutic target to mitigate ischemic injury during ex vivo hypothermic perfusion of kidneys from DCD rats. By targeting PCSK9, we aimed to enhance kidney conditioning and improve organ viability.

We demonstrated that the administration of the PCSK9 inhibitor PEP 2-8 during pre-transplant conditioning phase leads to a significant downregulation of PCSK9 gene expression. This molecular change was associated with tangible benefits, including robust protection of renal tissue from ischemic damage, preservation of tubular proliferation, a reduction in apoptosis, and attenuation of oxidative stress.

In a previous study, we reported that IRI in rats increased PCSK9 expression at both the gene and protein levels[37]. The current study, showing that PEP 2-8 treatment can reduce PCSK9 transcription, even after 6 hours of cold ischemia. This suggest a novel mechanism by which PEP 2-8 may confer protection against ischemic damage, potentially through direct gene regulation, although off-target effects cannot be ruled out. Our results are consistent with those of Schreckenberg et al. who showed that PCSK9 gene deletion, rather than protein inhibition, significantly reduced cardiac infarct size in an animal model of myocardial infarction[76]. A key finding of our study, is that PEP 2-8 treatment significantly decreased the tubular ischemic injury score. Kidneys conditioned with PEP 2-8 retained a higher percentage of normal tubules and exhibited a lower rate of necrosis compared to controls, indicating reduced cellular damage and better preservation of structural integrity. This protective effect extends to programmed cell death, as PCSK9 is known to activate apoptotic signaling pathways during ischemia[49–51,54]. In our model, the observed reduction in apoptosis in the treated group appears to be mediated by the caspase-3 signaling pathway. This aligns with in vitro studies, demonstrating that PCSK9 silencing inhibits in oxidized LDL-stimulated HUVECs the caspase-9-caspase-3 signaling pathway, thereby reducing cell damage[86].

Recent studies have also highlighted the role of PCSK9 in promoting oxidative stress, often by inducing NADPH oxidase expression[60,87,88]. Our findings support this association, as PEP 2-8 treatment reduced protein tyrosine nitration and downregulated NOX4, a key member of the NADPH oxidase family implicated in mitochondrial oxidative stress and the pathogenesis of various renal diseases[85,89,90]. This antioxidant effect is consistent with the findings of Liu et al., who demonstrated that PEP 2-8 reduced NOX4 expression and pro-inflammatory cytokine levels in a murine model of atherosclerosis[91]. The antioxidant properties of PCSK9 inhibition have also been confirmed in other models, including human studies on atherosclerosis-related vascular damage and in rats with post-alcoholic liver fibrosis treated with monoclonal antibodies[92–95].

To further investigate the molecular effects of PCSK9 inhibition during organ preservation, we conducted untargeted metabolomic profiling, identifying 167 biochemical compounds. Although stress conditions were the primary driver of metabolic changes, treatment with PEP 2-8 was linked to significant reductions in five metabolites associated to oxidative stress: 2-oxobutyrate, sarcosine, L-carnosine, dimethylamine, and biliverdin.

2-oxobutyrate, an α-keto acid generated by homocysteine metabolism, accumulates when methionine synthase activity is impaired by oxidative stress, reflecting a metabolic shift toward glutathione (GSH) synthesis [96] (Fig. 14).

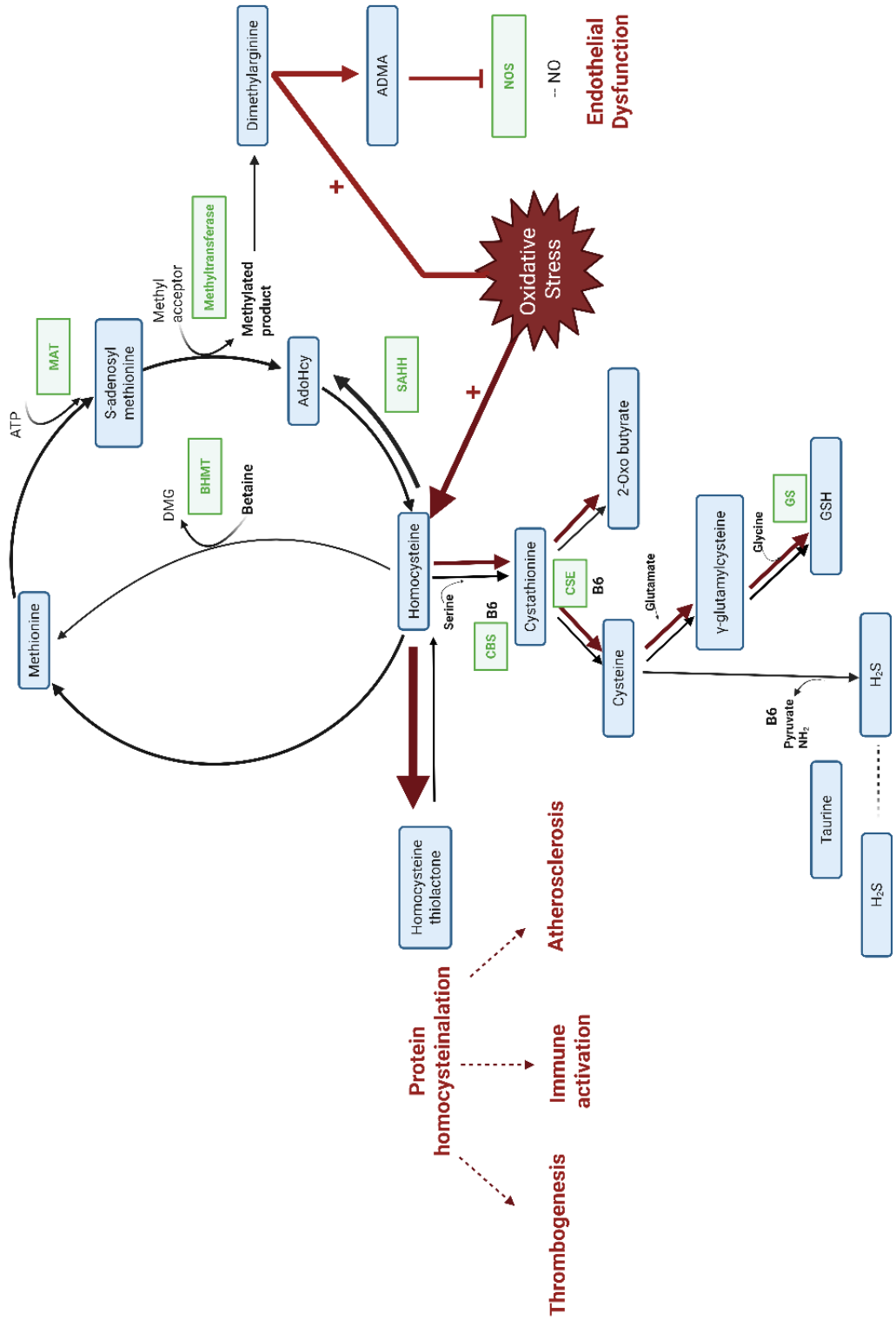


*Figure 14. Mechanisms Linking Oxidative Stress, Hyperhomocysteinemia, and Endothelial Dysfunction. (1) Oxidative stress impairs enzymes like methionine synthase, (2) reducing*

*remethylation of homocysteine to methionine, to produce (3) 2oxo butyrate, cysteine and (4) glutathione, an important antioxidant. Hyperhomocysteinemia accumulates in oxidized forms, (4) promoting oxidative stress leading to endothelial dysfunction, inflammation, and progression of cardiovascular diseases. (5) ADMA, an endogenous inhibitor of nitric oxide synthase (NOS), also increases during oxidative stress, reducing nitric oxide (NO) bioavailability, which impairs vascular function and promotes cardiovascular disease.*

*ADMA: asymmetric dimethylarginine, AdoHcy: S-adenosyl homocysteine, ATP: Adenosine Triphosphate, B6: vitamin B6, BHMT: betaine homocysteine methyltransferase, CBS: cystathionine βsynthase, CSE: cystathionine γ-lyase. GS: glutathione synthase, GSH: reduced glutathione, H2S: hydrogen sulfide, MAT: methionine adenosyl-transferase, NO: nitric oxide, NOS: nitric oxide synthase, SAHH: S-adenosyl homocysteine hydrolase. Minus (-) next to substance represents decreased level of substance; Plus (+) represents increased level of substance or increased enzyme activity. Red arrows represent the pathway triggered by oxidative stress. ("->" induction, "–|" inhibition). Created in BioRender. rampino, t. (2025).*

Dimethylamine is a toxic byproduct generated from the degradation of asymmetric dimethylarginine (ADMA) by dimethylarginine dimethyl-aminohydrolase (DDAH). Under oxidative stress, ADMA levels increase, impairing nitric oxide (NO) production and con-tributing to endothelial dysfunction[97–100] (Fig. 9). Supporting this, Moraes Ruberti et al., reported significantly elevated dimethylamine levels in rats following myocardial infarction[101]. Conversely, a reduction in dimethylamine suggests improved vascular homeostasis.

Sarcosine, a metabolite involved in choline metabolism, acts as a weak inhibitor of glycine transporters. Elevated sarcosine has been linked to decreased activity of sarcosine oxidase, an enzyme crucial for protecting cells from oxidative damage. Furthermore, acute sarcosine administration can exacerbate oxidative stress by inhibiting both mitochondrial and cytosolic energy enzymes[102,103].

L-carnosine is a well-known antioxidant, that functions either as a direct ROS scavenger or indirectly by enhancing the Nrf2 signaling pathway[104].

Finally, reduced biliverdin levels indicate decreased heme degradation, consistent with previous reports by Sajid et al., who observed altered heme oxygenase activity under hypoxic conditions[103–105].

Together, these metabolite changes reinforce the experimental evidence that PCSK9 inhibition enhances tissue resistance to ischemic injury by reducing oxidative stress.

Beyond its antioxidant effects, PEP 2-8 also appeared to improve energy metabolism in the renal perfusion model. This was demonstrated by increased ATP levels in kidney tissue and elevated glucose release in the effluent, indicating enhanced cellular energy production. Although cellular metabolism is significantly suppressed at 4°C in PEP 2-8 treated kidneys, it does not completely stop. This residual metabolic activity likely allows processes such as glycogenolysis, the breakdown of stored glycogen into glucose, to continue to some extent.

Furthermore, the reduction in oxidative stress markers suggests decreased cellular damage and more efficient cellular function.

Taken together, our findings indicate that PCSK9 inhibition supports renal energy metabolism by promoting ATP synthesis and limiting oxidative stress.

## 5.1. Limitations and strengths of the study

While this study provides valuable insights, several limitations must be acknowledged. First, the observation period was limited to six hours, which does not reflect the prolonged cold ischemia times typically experienced in human kidney transplantation, often lasting 24 to 36 hours. As a result, the experimental conditions may not fully capture the range or severity of injury seen in clinical practice.

Additionally, the study did not examine different doses or administration schedules of PEP 2-8, leaving open the possibility that alternative regimens could yield different or enhanced effects. The investigation was also restricted to the pre-reperfusion phase, so the potential benefits or limitations of administering PEP 2-8 during

reperfusion or trans-plantation, when oxidative stress and tissue injury peak, remain unknown.

Finally, the translational relevance of these findings to human kidney transplantation is uncertain. Variations in human physiology, ischemia duration, and clinical factors necessitate caution in directly extrapolating these experimental results to patient care.

Despite these limitations, our study highlights a novel application of PCSK9 inhibitors as a promising therapeutic strategy for various ischemic conditions, with potential for integration into pre-transplant organ conditioning protocols.

Improving the functional preservation of marginal kidneys could significantly expand the donor pool, carrying important implications for transplant programs worldwide. Increasing the availability of transplantable kidneys may help reduce waiting times and decrease reliance on dialysis, ultimately enhancing patient survival and quality of life. Given that kidney transplant recipients generally experience substantially better outcomes than those remaining on dialysis, interventions like PEP 2-8 could play a meaningful role in public health efforts to improve transplantation outcomes.

Moreover, the protective effects of PEP 2-8 may extend beyond kidney transplantation, offering potential benefits in other clinical scenarios marked by ischemia-reperfusion in-jury.

***References***


1. Bon D, Chatauret N, Giraud S, Thuillier R, Favreau F, Hauet T. New strategies to optimize kidney recovery and preservation in transplantation. *Nat Rev Nephrol*. 2012;8(6):339-347. doi:10.1038/nrneph.2012.83

2. Padilla S. 2025 International Registry in Organ Donation and Transplantation. Published online 2025.

3. Ariyamuthu VK, Qannus AA, Tanriover B. How do we increase deceased donor kidney utilization and reduce discard? *Curr Opin Organ Transplant*. 2025;30(3):215-221. doi:10.1097/MOT.0000000000001210

4. Noble J, Jouve T, Malvezzi P, Süsal C, Rostaing L. Transplantation of Marginal Organs: Immunological Aspects and Therapeutic Perspectives in Kidney Transplantation. *Front Immunol*. 2019;10:3142. doi:10.3389/fimmu.2019.03142

5. Franzin R, Stasi A, Fiorentino M, et al. Renal Delivery of Pharmacologic Agents During Machine Perfusion to Prevent Ischaemia-Reperfusion Injury: From Murine Model to Clinical Trials. *Front Immunol*. 2021;12. doi:10.3389/fimmu.2021.673562

6. Eltzschig HK, Eckle T. Ischemia and reperfusion--from mechanism to translation. *Nat Med*. 2011;17(11):1391-1401. doi:10.1038/nm.2507

7. Cowled P, Fitridge R. Pathophysiology of Reperfusion Injury. In: Fitridge R, Thompson M, eds. *Mechanisms of Vascular Disease: A Reference Book for Vascular Specialists*. University of Adelaide Press; 2011. Accessed September 10, 2025. http://www.ncbi.nlm.nih.gov/books/NBK534267/

8. Zhao H, Alam A, Soo AP, George AJT, Ma D. Ischemia-Reperfusion Injury Reduces Long Term Renal Graft Survival: Mechanism and Beyond. *EBioMedicine*. 2018;28:31-42. doi:10.1016/j.ebiom.2018.01.025

9. Kezic A, Spasojevic I, Lezaic V, Bajcetic M. Mitochondria-Targeted Antioxidants: Future Perspectives in Kidney Ischemia Reperfusion Injury. *Oxid Med Cell Longev*. 2016;2016:2950503. doi:10.1155/2016/2950503

10. Ponticelli C. Ischaemia-reperfusion injury: a major protagonist in kidney transplantation. *Nephrol Dial Transplant Off Publ Eur Dial Transpl Assoc - Eur Ren Assoc*. 2014;29(6):1134-1140. doi:10.1093/ndt/gft488

11. Lasorsa F, Rutigliano M, Milella M, et al. Ischemia-Reperfusion Injury in Kidney Transplantation: Mechanisms and Potential Therapeutic Targets. *Int J Mol Sci*. 2024;25(8):4332. doi:10.3390/ijms25084332

12. Salvadori M, Rosso G, Bertoni E. Update on ischemia-reperfusion injury in kidney transplantation: Pathogenesis and treatment. *World J Transplant*. 2015;5(2):52-67. doi:10.5500/wjt.v5.i2.52

13. Devarajan P. Update on mechanisms of ischemic acute kidney injury. *J Am Soc Nephrol JASN*. 2006;17(6):1503-1520. doi:10.1681/ASN.2006010017

14. Nieuwenhuijs-Moeke GJ, Pischke SE, Berger SP, et al. Ischemia and Reperfusion Injury in Kidney Transplantation: Relevant Mechanisms in Injury and Repair. *J Clin Med*. 2020;9(1):253. doi:10.3390/jcm9010253

15. Zhao H, Kilgas S, Alam A, Eguchi S, Ma D. The Role of Extracellular Adenosine Triphosphate in Ischemic Organ Injury. *Crit Care Med*. 2016;44(5):1000-1012. doi:10.1097/CCM.0000000000001603

16. Fujii K, Kubo A, Miyashita K, et al. Xanthine oxidase inhibitor ameliorates postischemic renal injury in mice by promoting resynthesis of adenine nucleotides. *JCI Insight*. 2019;4(22):e124816, 124816. doi:10.1172/jci.insight.124816

17. Malek M, Nematbakhsh M. Renal ischemia/reperfusion injury; from pathophysiology to treatment. *J Ren Inj Prev*. 2015;4(2):20-27. doi:10.12861/jrip.2015.06

18. Sharfuddin AA, Molitoris BA. Pathophysiology of ischemic acute kidney injury. *Nat Rev Nephrol*. 2011;7(4):189-200. doi:10.1038/nrneph.2011.16

19. Farías JG, Herrera EA, Carrasco-Pozo C, et al. Pharmacological models and approaches for pathophysiological conditions associated with hypoxia and oxidative stress. *Pharmacol Ther*. 2016;158:1-23. doi:10.1016/j.pharmthera.2015.11.006

20. McCord JM. Oxygen-derived free radicals in postischemic tissue injury. *N Engl J Med*. 1985;312(3):159-163. doi:10.1056/NEJM198501173120305

21. Paller MS, Hoidal JR, Ferris TF. Oxygen free radicals in ischemic acute renal failure in the rat. *J Clin Invest*. 1984;74(4):1156-1164. doi:10.1172/JCI111524

22. Collard CD, Gelman S. Pathophysiology, clinical manifestations, and prevention of ischemia-reperfusion injury. *Anesthesiology*. 2001;94(6):1133-1138. doi:10.1097/00000542-200106000-00030

23. Kosieradzki M, Rowiński W. Ischemia/reperfusion injury in kidney transplantation: mechanisms and prevention. *Transplant Proc*. 2008;40(10):3279-3288. doi:10.1016/j.transproceed.2008.10.004

24. Ghoneima AS, Sousa Da Silva RX, Gosteli MA, Barlow AD, Kron P. Outcomes of Kidney Perfusion Techniques in Transplantation from Deceased Donors: A Systematic Review and Meta-Analysis. *J Clin Med*. 2023;12(12):3871. doi:10.3390/jcm12123871

25. Tatsis V, Dounousi E, Mitsis M. Hypothermic Machine Perfusion of Kidney Transplant: A Mini-Review. *Transplant Proc*. 2021;53(9):2793-2796. doi:10.1016/j.transproceed.2021.09.011

26. Hosgood SA, Brown RJ, Nicholson ML. Advances in Kidney Preservation Techniques and Their Application in Clinical Practice. *Transplantation*. 2021;105(11):e202-e214. doi:10.1097/TP.0000000000003679

27. Ramos P, Williams P, Salinas J, et al. Abdominal Organ Preservation Solutions in the Age of Machine Perfusion. *Transplantation*. 2023;107(2):326-340. doi:10.1097/TP.0000000000004269

28. Kataria A, Magoon S, Makkar B, Gundroo A. Machine perfusion in kidney transplantation. *Curr Opin Organ Transplant*. 2019;24(4):378-384. doi:10.1097/MOT.0000000000000675

29. Moers C, Smits JM, Maathuis MHJ, et al. Machine perfusion or cold storage in deceased-donor kidney transplantation. *N Engl J Med*. 2009;360(1):7-19. doi:10.1056/NEJMoa0802289

30. Hosgood SA, Hoff M, Nicholson ML. Treatment of transplant kidneys during machine perfusion. *Transpl Int Off J Eur Soc Organ Transplant*. 2021;34(2):224-232. doi:10.1111/tri.13751

31. von Horn C, Zlatev H, Kaths M, Paul A, Minor T. Controlled Oxygenated Rewarming Compensates for Cold Storage-induced Dysfunction in Kidney Grafts. *Transplantation*. 2022;106(5):973-978. doi:10.1097/TP.0000000000003854

32. Tingle SJ, Thompson ER, Figueiredo RS, et al. Normothermic and hypothermic machine perfusion preservation versus static cold storage for deceased donor kidney transplantation. *Cochrane Database Syst Rev*. 2024;7(7):CD011671. doi:10.1002/14651858.CD011671.pub3

33. Unes M, Kurashima K, Caliskan Y, Portz E, Jain A, Nazzal M. Normothermic ex vivo perfusion of deceased donor kidneys and its clinical potential in kidney transplantation outcomes. *Int J Artif Organs*. 2023;46(12):618-628. doi:10.1177/03913988231207719

34. Esposito P, Grosjean F, Rampino T, et al. Costimulatory pathways in kidney transplantation: pathogenetic role, clinical significance and new therapeutic

opportunities. *Int Rev Immunol*. 2014;33(3):212-233. doi:10.3109/08830185.2013.829470

35. Zhang M, Liu Q, Meng H, et al. Ischemia-reperfusion injury: molecular mechanisms and therapeutic targets. *Signal Transduct Target Ther*. 2024;9(1):12. doi:10.1038/s41392-023-01688-x

36. Barisione C, Verzola D, Garibaldi S, et al. Renal Ischemia/Reperfusion Early Induces Myostatin and PCSK9 Expression in Rat Kidneys and HK-2 Cells. *Int J Mol Sci*. 2021;22(18):9884. doi:10.3390/ijms22189884

37. Ortona S, Barisione C, Ferrari PF, Palombo D, Pratesi G. PCSK9 and Other Metabolic Targets to Counteract Ischemia/Reperfusion Injury in Acute Myocardial Infarction and Visceral Vascular Surgery. *J Clin Med*. 2022;11(13):3638. doi:10.3390/jcm11133638

38. Huang G, Lu X, Duan Z, et al. PCSK9 Knockdown Can Improve Myocardial Ischemia/Reperfusion Injury by Inhibiting Autophagy. *Cardiovasc Toxicol*. 2022;22(12):951-961. doi:10.1007/s12012-022-09771-5

39. Huang G, Lu X, Zhou H, et al. PCSK9 inhibition protects against myocardial ischemia-reperfusion injury via suppressing autophagy. *Microvasc Res*. 2022;142:104371. doi:10.1016/j.mvr.2022.104371

40. Andreadou I, Tsoumani M, Vilahur G, et al. PCSK9 in Myocardial Infarction and Cardioprotection: Importance of Lipid Metabolism and Inflammation. *Front Physiol*. 2020;11:602497. doi:10.3389/fphys.2020.602497

41. Guo H, Li W, Yang Z, Xing X. E3 ubiquitin ligase MARCH1 reduces inflammation and pyroptosis in cerebral ischemia-reperfusion injury via PCSK9 downregulation. *Mamm Genome Off J Int Mamm Genome Soc*. 2024;35(3):346-361. doi:10.1007/s00335-024-10055-2

42. Apaijai N, Moisescu DM, Palee S, et al. Pretreatment With PCSK9 Inhibitor Protects the Brain Against Cardiac Ischemia/Reperfusion Injury Through a Reduction of Neuronal Inflammation and Amyloid Beta Aggregation. *J Am Heart Assoc*. 2019;8(2):e010838. doi:10.1161/JAHA.118.010838

43. Pu S, Jia C, Li Z, Zang Y. Protective Mechanism of Proprotein Convertase Subtilisin-Like Kexin Type 9 Inhibitor on Rats with Middle Cerebral Artery Occlusion-Induced Cerebral Ischemic Infarction. *Comput Intell Neurosci*. 2022;2022:4964262. doi:10.1155/2022/4964262

44. Seidah NG, Prat A. The Multifaceted Biology of PCSK9. *Endocr Rev*. 2022;43(3):558-582. doi:10.1210/endrev/bnab035

45. Shapiro MD, Fazio S. Dyslipidaemia: The PCSK9 adventure - humanizing extreme LDL lowering. *Nat Rev Cardiol*. 2017;14(6):319-320. doi:10.1038/nrcardio.2017.66

46. Melendez QM, Krishnaji ST, Wooten CJ, Lopez D. Hypercholesterolemia: The role of PCSK9. *Arch Biochem Biophys*. 2017;625-626:39-53. doi:10.1016/j.abb.2017.06.001

47. Zaid A, Roubtsova A, Essalmani R, et al. Proprotein convertase subtilisin/kexin type 9 (PCSK9): hepatocyte-specific low-density lipoprotein receptor degradation and critical role in mouse liver regeneration. *Hepatol Baltim Md*. 2008;48(2):646-654. doi:10.1002/hep.22354

48. Targeting the peptidase PCSK9 to reduce cardiovascular risk: Implications for basic science and upcoming challenges - Nishikido - 2021 - British Journal of Pharmacology - Wiley Online Library. Accessed September 14, 2025. https://bpspubs.onlinelibrary.wiley.com/doi/10.1111/bph.14851

49. Lambert G, Sjouke B, Choque B, Kastelein JJP, Hovingh GK. The PCSK9 decade. *J Lipid Res*. 2012;53(12):2515-2524. doi:10.1194/jlr.R026658

50. Bao X, Liang Y, Chang H, et al. Targeting proprotein convertase subtilisin/kexin type 9 (PCSK9): from bench to bedside. *Signal Transduct Target Ther*. 2024;9(1):13. doi:10.1038/s41392-023-01690-3

51. Dutka M, Zimmer K, Ćwiertnia M, Ilczak T, Bobiński R. The role of PCSK9 in heart failure and other cardiovascular diseases-mechanisms of action beyond its effect on LDL cholesterol. *Heart Fail Rev*. 2024;29(5):917-937. doi:10.1007/s10741-024-10409-7

52. Wu C, Lin D, Ji J, Jiang Y, Jiang F, Wang Y. PCSK9 Inhibition Regulates Infarction-Induced Cardiac Myofibroblast Transdifferentiation via Notch1 Signaling. *Cell Biochem Biophys*. 2023;81(2):359-369. doi:10.1007/s12013-023-01136-1

53. Ma M, Hou C, Liu J. Effect of PCSK9 on atherosclerotic cardiovascular diseases and its mechanisms: Focus on immune regulation. *Front Cardiovasc Med*. 2023;10:1148486. doi:10.3389/fcvm.2023.1148486

54. Guo Y, Yan B, Tai S, Zhou S, Zheng XL. PCSK9: Associated with cardiac diseases and their risk factors? *Arch Biochem Biophys*. 2021;704:108717. doi:10.1016/j.abb.2020.108717

55. Xu Q, Zhao YM, He NQ, et al. PCSK9: A emerging participant in heart failure. *Biomed Pharmacother Biomedecine Pharmacother*. 2023;158:114106. doi:10.1016/j.biopha.2022.114106

56. Momtazi-Borojeni AA, Banach M, Ruscica M, Sahebkar A. The role of PCSK9 in NAFLD/NASH and therapeutic implications of PCSK9 inhibition. *Expert Rev Clin Pharmacol*. 2022;15(10):1199-1208. doi:10.1080/17512433.2022.2132229

57. Han L, Wu L, Yin Q, et al. A promising therapy for fatty liver disease: PCSK9 inhibitors. *Phytomedicine Int J Phytother Phytopharm*. 2024;128:155505. doi:10.1016/j.phymed.2024.155505

58. Ding Z, Pothineni NVK, Goel A, Lüscher TF, Mehta JL. PCSK9 and inflammation: role of shear stress, pro-inflammatory cytokines, and LOX-1. *Cardiovasc Res*. 2020;116(5):908-915. doi:10.1093/cvr/cvz313

59. Walley KR. Role of lipoproteins and proprotein convertase subtilisin/kexin type 9 in endotoxin clearance in sepsis. *Curr Opin Crit Care*. 2016;22(5):464-469. doi:10.1097/MCC.0000000000000351

60. Wang X, Li X, Liu S, et al. PCSK9 regulates pyroptosis via mtDNA damage in chronic myocardial ischemia. *Basic Res Cardiol*. 2020;115(6):66. doi:10.1007/s00395-020-00832-w

61. Zhang M, Chen Y, Qiu Y, et al. PCSK9 Promotes Hypoxia-Induced EC Pyroptosis by Regulating Smac Mitochondrion-Cytoplasm Translocation in Critical Limb Ischemia. *JACC Basic Transl Sci*. 2023;8(9):1060-1077. doi:10.1016/j.jacbts.2023.05.016

62. Ivan L, Uyy E, Suica VI, et al. Hepatic Alarmins and Mitochondrial Dysfunction under Residual Hyperlipidemic Stress Lead to Irreversible NAFLD. *J Clin Transl Hepatol*. 2023;11(2):284-294. doi:10.14218/JCTH.2022.00128

63. Wu D, Zhou Y, Pan Y, et al. Vaccine Against PCSK9 Improved Renal Fibrosis by Regulating Fatty Acid β-Oxidation. *J Am Heart Assoc*. 2020;9(1):e014358. doi:10.1161/JAHA.119.014358

64. Zhang Y, Wang Z, Jia C, et al. Blockade of Hepatocyte PCSK9 Ameliorates Hepatic Ischemia-Reperfusion Injury by Promoting Pink1-Parkin-Mediated Mitophagy. *Cell Mol Gastroenterol Hepatol*. 2024;17(1):149-169. doi:10.1016/j.jcmgh.2023.09.004

65. Amput P, Palee S, Arunsak B, et al. PCSK9 inhibitor and atorvastatin reduce cardiac impairment in ovariectomized prediabetic rats via improved mitochondrial function and Ca2+ regulation. *J Cell Mol Med*. 2020;24(16):9189-9203. doi:10.1111/jcmm.15556

66. Li X, Dai F, Wang H, et al. PCSK9 participates in oxidized-low density lipoprotein-induced myocardial injury through mitochondrial oxidative stress and Drp1-

mediated mitochondrial fission. *Clin Transl Med*. 2022;12(2):e729. doi:10.1002/ctm2.729

67. Ding Z, Liu S, Wang X, et al. Cross-Talk Between PCSK9 and Damaged mtDNA in Vascular Smooth Muscle Cells: Role in Apoptosis. *Antioxid Redox Signal*. 2016;25(18):997-1008. doi:10.1089/ars.2016.6631

68. Xu X, Cui Y, Cao L, Zhang Y, Yin Y, Hu X. PCSK9 regulates apoptosis in human lung adenocarcinoma A549 cells via endoplasmic reticulum stress and mitochondrial signaling pathways. *Exp Ther Med*. 2017;13(5):1993-1999. doi:10.3892/etm.2017.4218

69. Xu B, Li S, Fang Y, et al. Proprotein Convertase Subtilisin/Kexin Type 9 Promotes Gastric Cancer Metastasis and Suppresses Apoptosis by Facilitating MAPK Signaling Pathway Through HSP70 Up-Regulation. *Front Oncol*. 2020;10:609663. doi:10.3389/fonc.2020.609663

70. Xu R, Li T, Luo J, et al. PCSK9 increases vulnerability of carotid plaque by promoting mitochondrial dysfunction and apoptosis of vascular smooth muscle cells. *CNS Neurosci Ther*. 2024;30(2):e14640. doi:10.1111/cns.14640

71. Palee S, McSweeney CM, Maneechote C, et al. PCSK9 inhibitor improves cardiac function and reduces infarct size in rats with ischaemia/reperfusion injury: Benefits beyond lipid-lowering effects. *J Cell Mol Med*. 2019;23(11):7310-7319. doi:10.1111/jcmm.14586

72. Zhang Y, Eigenbrot C, Zhou L, et al. Identification of a small peptide that inhibits PCSK9 protein binding to the low density lipoprotein receptor. *J Biol Chem*. 2014;289(2):942-955. doi:10.1074/jbc.M113.514067

73. Huang L, Li Y, Cheng Z, Lv Z, Luo S, Xia Y. PCSK9 Promotes Endothelial Dysfunction During Sepsis Via the TLR4/MyD88/NF-κB and NLRP3 Pathways. *Inflammation*. 2023;46(1):115-128. doi:10.1007/s10753-022-01715-z

74. Percie du Sert N, Hurst V, Ahluwalia A, et al. The ARRIVE guidelines 2.0: Updated guidelines for reporting animal research. *PLoS Biol*. 2020;18(7):e3000410. doi:10.1371/journal.pbio.3000410

75. Grignano MA, Bruno S, Viglio S, et al. CD73-Adenosinergic Axis Mediates the Protective Effect of Extracellular Vesicles Derived from Mesenchymal Stromal Cells on Ischemic Renal Damage in a Rat Model of Donation after Circulatory Death. *Int J Mol Sci*. 2022;23(18):10681. doi:10.3390/ijms231810681

76. Schreckenberg R, Wolf A, Szabados T, et al. Proprotein Convertase Subtilisin Kexin Type 9 (PCSK9) Deletion but Not Inhibition of Extracellular PCSK9 Reduces

Infarct Sizes Ex Vivo but Not In Vivo. *Int J Mol Sci*. 2022;23(12):6512. doi:10.3390/ijms23126512

77. Crowe AR, Yue W. Semi-quantitative Determination of Protein Expression using Immunohistochemistry Staining and Analysis: An Integrated Protocol. *Bio-Protoc*. 2019;9(24):e3465. doi:10.21769/BioProtoc.3465

78. Bustin SA, Benes V, Garson JA, et al. The MIQE guidelines: minimum information for publication of quantitative real-time PCR experiments. *Clin Chem*. 2009;55(4):611-622. doi:10.1373/clinchem.2008.112797

79. Bustin SA. Improving the quality of quantitative polymerase chain reaction experiments: 15 years of MIQE. *Mol Aspects Med*. 2024;96:101249. doi:10.1016/j.mam.2024.101249

80. Lefort G, Liaubet L, Marty-Gasset N, Canlet C, Vialaneix N, Servien R. Joint Automatic Metabolite Identification and Quantification of a Set of 1H NMR Spectra. *Anal Chem*. 2021;93(5):2861-2870. doi:10.1021/acs.analchem.0c04232

81. Lefort G, Liaubet L, Canlet C, et al. ASICS: an R package for a whole analysis workflow of 1D 1H NMR spectra. *Bioinforma Oxf Engl*. 2019;35(21):4356-4363. doi:10.1093/bioinformatics/btz248

82. How the 1D-NOESY suppresses solvent signal in metabonomics NMR spectroscopy: An examination of the pulse sequence components and evolution - Mckay - 2011 - Concepts in Magnetic Resonance Part A - Wiley Online Library. Accessed September 12, 2025. https://onlinelibrary.wiley.com/doi/10.1002/cmr.a.20223

83. Silva JG, Tavares L, Belew GD, et al. Impact of High-Fat Diet-induced Metabolic Dysfunction-associated Steatotic Liver Disease on Heart, Kidney, and Skeletal Muscle Metabolomes in Wild-Type Mice. *J Proteome Res*. 2025;24(5):2491-2504. doi:10.1021/acs.jproteome.5c00040

84. Debik J, Sangermani M, Wang F, Madssen TS, Giskeødegård GF. Multivariate analysis of NMR-based metabolomic data. *NMR Biomed*. 2022;35(2):e4638. doi:10.1002/nbm.4638

85. Bedard K, Krause KH. The NOX family of ROS-generating NADPH oxidases: physiology and pathophysiology. *Physiol Rev*. 2007;87(1):245-313. doi:10.1152/physrev.00044.2005

86. Wu CY, Tang ZH, Jiang L, Li XF, Jiang ZS, Liu LS. PCSK9 siRNA inhibits HUVEC apoptosis induced by ox-LDL via Bcl/Bax-caspase9-caspase3 pathway. *Mol Cell Biochem*. 2012;359(1-2):347-358. doi:10.1007/s11010-011-1028-6

87. Jaén RI, Povo-Retana A, Rosales-Mendoza C, et al. Functional Crosstalk between PCSK9 Internalization and Pro-Inflammatory Activation in Human Macrophages: Role of Reactive Oxygen Species Release. *Int J Mol Sci*. 2022;23(16):9114. doi:10.3390/ijms23169114

88. Ding Z, Liu S, Wang X, et al. Hemodynamic shear stress via ROS modulates PCSK9 expression in human vascular endothelial and smooth muscle cells and along the mouse aorta. *Antioxid Redox Signal*. 2015;22(9):760-771. doi:10.1089/ars.2014.6054

89. Holterman CE, Read NC, Kennedy CRJ. Nox and renal disease. *Clin Sci Lond Engl 1979*. 2015;128(8):465-481. doi:10.1042/CS20140361

90. Thamilselvan V, Menon M, Thamilselvan S. Oxalate-induced activation of PKC-α and -δ regulates NADPH oxidase-mediated oxidative injury in renal tubular epithelial cells. *Am J Physiol-Ren Physiol*. 2009;297(5):F1399-F1410. doi:10.1152/ajprenal.00051.2009

91. Liu S, Wu J, Stolarz A, et al. PCSK9 attenuates efferocytosis in endothelial cells and promotes vascular aging. *Theranostics*. 2023;13(9):2914-2929. doi:10.7150/thno.83914

92. Safaeian L, Mirian M, Bahrizadeh S. Evolocumab, a PCSK9 inhibitor, protects human endothelial cells against H2O2-induced oxidative stress. *Arch Physiol Biochem*. 2022;128(6):1681-1686. doi:10.1080/13813455.2020.1788605

93. Lankin VZ, Tikhaze AK, Viigimaa M, Chazova IE. PCSK9 Inhibitor causes a decrease in the level of oxidatively modified low-density lipoproteins in patients with coronary artery diseases. *Ter Arkh*. 2018;90(9):27-30. doi:10.26442/terarkh201890927-30

94. Cammisotto V, Baratta F, Castellani V, et al. Proprotein Convertase Subtilisin Kexin Type 9 Inhibitors Reduce Platelet Activation Modulating ox-LDL Pathways. *Int J Mol Sci*. 2021;22(13):7193. doi:10.3390/ijms22137193

95. Lee JS, Mukhopadhyay P, Matyas C, et al. PCSK9 inhibition as a novel therapeutic target for alcoholic liver disease. *Sci Rep*. 2019;9(1):17167. doi:10.1038/s41598-019-53603-6

96. Bajic Z, Sobot T, Skrbic R, et al. Homocysteine, Vitamins B6 and Folic Acid in Experimental Models of Myocardial Infarction and Heart Failure-How Strong Is That Link? *Biomolecules*. 2022;12(4):536. doi:10.3390/biom12040536

97. Oliva-Damaso E, Oliva-Damaso N, Rodriguez-Esparragon F, et al. Asymmetric (ADMA) and Symmetric (SDMA) Dimethylarginines in Chronic Kidney Disease: A Clinical Approach. *Int J Mol Sci*. 2019;20(15):3668. doi:10.3390/ijms20153668

98. Kurata H, Fujii T, Tsutsui H, et al. Renoprotective effects of l-carnosine on ischemia/reperfusion-induced renal injury in rats. *J Pharmacol Exp Ther*. 2006;319(2):640-647. doi:10.1124/jpet.106.110122

99. Jankowski J, Westhof T, Vaziri ND, Ingrosso D, Perna AF. Gases as Uremic Toxins: Is There Something in the Air? *Semin Nephrol*. 2014;34(2):135-150. doi:10.1016/j.semnephrol.2014.02.006

100. Blackwell S. The biochemistry, measurement and current clinical significance of asymmetric dimethylarginine. *Ann Clin Biochem*. 2010;47(Pt 1):17-28. doi:10.1258/acb.2009.009196

101. Ruberti OM, Sousa AS, Viana LR, et al. Aerobic training prevents cardiometabolic changes triggered by myocardial infarction in ovariectomized rats. *J Cell Physiol*. 2021;236(2):1105-1115. doi:10.1002/jcp.29919

102. Joncquel M, Labasque J, Demaret J, et al. Targeted Metabolomics Analysis Suggests That Tacrolimus Alters Protection against Oxidative Stress. *Antioxid Basel Switz*. 2023;12(7):1412. doi:10.3390/antiox12071412

103. de Andrade RB, Gemelli T, Rojas DB, et al. Evaluation of Oxidative Stress Parameters and Energy Metabolism in Cerebral Cortex of Rats Subjected to Sarcosine Administration. *Mol Neurobiol*. 2017;54(6):4496-4506. doi:10.1007/s12035-016-9984-1

104. Hipkiss AR. Energy metabolism, proteotoxic stress and age-related dysfunction – Protection by carnosine. *Mol Aspects Med*. 2011;32(4):267-278. doi:10.1016/j.mam.2011.10.004